Report

Neuron

Thalamus Modulates Consciousness via Layer-Specific Control of Cortex

Highlights

- Central lateral thalamic stimulation arouses macaques from stable anesthesia
- Thalamic and deep-layer cortical spiking correlate with consciousness level
- Consciousness depends on feedforward, feedback, and intracolumnar signaling
- Pathway-specific signaling operates at alpha and gamma during consciousness

Authors

Michelle J. Redinbaugh, Jessica M. Phillips, Niranjan A. Kambi, ..., Mohsen Afrasiabi, Aeyal Raz, Yuri B. Saalmann

Correspondence

mredinbaugh@wisc.edu (M.J.R.), saalmann@wisc.edu (Y.B.S.)

In Brief

Redinbaugh et al. demonstrate neural correlates of consciousness, consistent in wakefulness and stimulation-induced arousal, which break down during anesthesia and sleep. The authors conclude that activity in central lateral thalamus and cortical deep layers is vital for consciousness, influencing feedforward, feedback, and intracolumnar processes.

Redinbaugh et al., 2020, Neuron *106*, 66–75
April 8, 2020
https://doi.org/10.1016/j.neuron.2020.01.005

CellPress

CellPress

Neuron
Report

Thalamus Modulates Consciousness via Layer-Specific Control of Cortex

Michelle J. Redinbaugh,[1,*] Jessica M. Phillips,[1] Niranjan A. Kambi,[1] Sounak Mohanta,[1] Samantha Andryk,[1] Gaven L. Dooley,[1] Mohsen Afrasiabi,[1] Aeyal Raz,[2,3,5] and Yuri B. Saalmann[1,4,5,6,*]
[1]Department of Psychology, University of Wisconsin-Madison, Madison, WI 53706, USA
[2]Department of Anesthesiology, Rambam Health Care Campus, Haifa 3109601, Israel
[3]Ruth and Bruce Rappaport Faculty of Medicine, Technion – Israel Institute of Technology, Haifa 3200003, Israel
[4]Wisconsin National Primate Research Center, Madison, WI 53715, USA
[5]These authors contributed equally
[6]Lead Contact
*Correspondence: mredinbaugh@wisc.edu (M.J.R.), saalmann@wisc.edu (Y.B.S.)
https://doi.org/10.1016/j.neuron.2020.01.005

SUMMARY

Functional MRI and electrophysiology studies suggest that consciousness depends on large-scale thalamocortical and corticocortical interactions. However, it is unclear how neurons in different cortical layers and circuits contribute. We simultaneously recorded from central lateral thalamus (CL) and across layers of the frontoparietal cortex in awake, sleeping, and anesthetized macaques. We found that neurons in thalamus and deep cortical layers are most sensitive to changes in consciousness level, consistent across different anesthetic agents and sleep. Deep-layer activity is sustained by interactions with CL. Consciousness also depends on deep-layer neurons providing feedback to superficial layers (not to deep layers), suggesting that long-range feedback and intracolumnar signaling are important. To show causality, we stimulated CL in anesthetized macaques and effectively restored arousal and wake-like neural processing. This effect was location and frequency specific. Our findings suggest layer-specific thalamocortical correlates of consciousness and inform how targeted deep brain stimulation can alleviate disorders of consciousness.

INTRODUCTION

Consciousness is the capacity to experience one's environment and internal states. The minimal mechanisms that are sufficient for this experience, the neural correlates of consciousness (NCC), are much debated (Dehaene and Changeux, 2011; Friston, 2010; Lamme, 2006; Oizumi et al., 2014). Nonetheless, major theories of consciousness emphasize the importance of recurrent activity and interaction between neurons. This can take the form of communication between brain areas along feedforward and feedback pathways and intracolumnar communication within a cortical area.

Feedforward pathways carry sensory information from superficial layers to superficial and middle layers of higher-order cortical areas, whereas feedback pathways carry priorities and predictions from deep layers to either superficial or deep layers of lower-order cortical areas (Markov et al., 2014; Mejias et al., 2016). Reports of the contribution of feedforward (Maksimow et al., 2014; Sanders et al., 2018; van Vugt et al., 2018) and feedback (Boly et al., 2011; Lee et al., 2009, 2013; Raz et al., 2014; Uhrig et al., 2018) pathways to consciousness have varied. However, previous studies did not have the spatial resolution to determine transmission along paths between specific layers—in particular, whether feedback paths to superficial or deep cortical layers, or both, contribute to consciousness.

Available evidence suggests that changes in the level of consciousness differentially influences activity in cortical layers. Non-rapid eye movement (NREM) sleep reduces spiking activity in deep layers of the primary visual cortex (V1) in mice and cats (Livingstone and Hubel, 1981; Senzai et al., 2019), as well as interactions between the superficial and deep layers of V1 (Senzai et al., 2019). NREM sleep in mice (Funk et al., 2016) and isoflurane anesthesia in ferrets (Sellers et al., 2013) also changes local field potentials (LFPs) differentially across layers. It is unclear how changes in consciousness influence individual neurons across layers, and their interaction, in the higher-order cortex.

Reciprocally connected with the higher-order cortex, higher-order thalamic areas facilitate cortical communication (Saalmann et al., 2012; Schmitt et al., 2017; Theyel et al., 2010) and could thus play a role in modulating corticocortical interaction across different conscious states. Changes in consciousness level broadly influence thalamic activity and thalamocortical interactions (Baker et al., 2014; Contreras et al., 1997; Jones, 2009; Llinás et al., 1998). However, the central lateral thalamus (CL) may have a special relation to consciousness. CL damage is linked to disorders of consciousness (Schiff, 2008). Anatomically, CL receives input from the brainstem reticular activating system. It also projects to superficial layers and reciprocally connects with deep layers of the frontoparietal cortex (Kaufman and Rosenquist, 1985; Purpura and Schiff, 1997; Towns et al.,

1990). Thus, CL is well positioned to influence information flow between cortical layers and areas. Deep brain stimulation of the central thalamus increased responsiveness in a minimally conscious patient (Schiff et al., 2007), and central thalamic stimulation improved the performance of a vigilance task in healthy macaques (Baker et al., 2016). Although thalamocortical mechanisms of such effects have been proposed (Jones, 2009; Llinás et al., 1998; Purpura and Schiff, 1997), experimental evidence is lacking. Based on its connectivity, we hypothesized that CL influences feedforward, feedback, and intracolumnar cortical processes to regulate information flow, and thus, consciousness.

To resolve the contributions of corticocortical and thalamocortical paths to the NCC, we used linear multi-electrode arrays to record spikes and LFPs simultaneously from the right frontal eye field (FEF); the lateral intraparietal area (LIP; frontoparietal areas implicated in awareness) (Wardak et al., 2002, 2006); and interconnected CL in two macaques during task-free wakefulness, NREM sleep, and general anesthesia (isoflurane, propofol). After characterizing thalamocortical network activity under anesthesia, we electrically stimulated the thalamus, reliably inducing arousal. We report layer-specific NCC in frontoparietal cortex and cortico-CL pathways.

RESULTS

Gamma-Frequency CL Stimulation Increased Consciousness Level

After maintaining stable anesthesia (arousal score 0–1) for at least 2 h while recording neural activity, we evaluated the signs of arousal before, during, and after stimulation using a customized scale similar to clinical metrics (STAR Methods) and performed statistical analyses using general linear models (STAR Methods; Tables S1–S4). Across 261 stimulation blocks, thalamic stimulation significantly increased arousal relative to pre- ($F = 119.28$, $n = 261$, $p < 1.0 \times 10^{-10}$) and post-conditions ($F = 124.64$, $n = 261$, $p < 1.0 \times 10^{-10}$), even when accounting for differences in dose and anesthetic (Figures 1A, 1B, and S1A–S1C). Behavioral changes (Figure 1A) were time locked to stimulation: monkeys opened their eyes with wake-like occasional blinks, performed full reaches and withdrawals with forelimbs (ipsi- or contralateral), made facial and body movements, showed increased reactivity (palpebral reflex, toe-pinch withdrawal), and had altered vital signs (respiration rate, heart rate). The reconstruction of electrode tracks placed effective stimulations (arousal score ≥ 3) near the center of CL (Figures 1C–1F). Euclidian proximity of the stimulation array to CL significantly predicted changes in arousal (Figures S1G–S1I; $T = -3.39$, $n = 225$, $p = 0.00082$); when systematically varying array depth, proximity to the CL center showed a significant quadratic relation with arousal ($T = -2.92$, $n = 225$, $p = 0.00393$; Figures 1F and S1D–S1F). Effective stimulation sites remained so on separate recording days and with different anesthetics (Figure 1G). Stimulation effectiveness depended on frequency (Figures 1G and 1H). At effective sites, only 50-Hz stimulations reliably increased arousal ($T = 3.91$, $n = 44$, $p = 0.00035$). These results show that CL stimulation can rouse animals from stable, anesthetized states. This allowed us to zero in on NCCs, identified here as activity differences between wakefulness and anesthesia, which are selectively restored by effective (arousal score ≥ 3, $n = 55$, mean = 4.70, SD = 1.70) relative to ineffective (arousal score < 3, $n = 171$, mean = 0.77, SD = 0.74) 50-Hz stimulations.

Consciousness Level Modulated Spike Rate and Timing in Deep Cortical Layers and CL

We recorded 845 neurons across 3 brain areas (FEF, LIP, CL) during 4 states (wake, sleep, isoflurane, propofol; Figure 2). Wake and anesthesia data derived from separate sessions, whereas the same neurons yielded sleep and wake data. This included a subset of CL neurons with a relatively high firing rate (~40–50 Hz; Figures S2E and S2F), similar to neurons reported in cats (Glenn and Steriade, 1982; Steriade et al., 1993). Thalamic neurons showed state-dependent spike rate and bursting activity (Figures 2C and 2D). CL neurons recorded during anesthesia ($T = -4.67$, $n = 282$, $p = 3.0 \times 10^{-5}$) and NREM sleep ($F = 16.40$, $n = 83$, $p = 0.001$) had significantly lower spike rates than during wakefulness. Isoflurane and propofol effects were not significantly different (Figure S2A). Relative to wakefulness, CL neurons also increased bursting during anesthesia (Figures 2D and S2G; $T = 2.27$, $n = 172$, $p = 0.024$) and sleep ($F = 7.11$, $n = 121$, $p = 0.0095$).

We localized cortical neurons to superficial, middle, or deep layers using current source density (CSD) responses to sounds in the passive oddball paradigm (Figures 2A and 2B). Only deep neurons showed state-dependent activity (Figures 2E–2H). Firing rates during sleep were significantly lower than wakefulness; the state-by-layer interaction was significant in both FEF ($F = 15.17$, $n = 101$, $p = 0.008$) and LIP ($F = 7.70$, $n = 98$, $p = 0.031$). Similarly, firing rates during anesthesia were lower than during wakefulness; state-by-layer interactions in FEF ($T = 3.05$, $n = 281$, $p = 0.013$) and LIP ($T = 3.79$, $n = 282$, $p = 0.001$) were significant. Only deep neurons increased bursting during anesthesia, evidenced by significant state-by-layer interaction (Figure 2E; $T = 2.12$, $n = 285$, $p = 0.035$). Isoflurane and propofol yielded similar results (Figures S2B–S2D). Effective 50-Hz thalamic stimulation countered anesthesia effects in deep cortical layers of the LIP (Figures 2I–2K); the 4-way interaction of stimulation epoch, effectiveness, layer, and area was significant ($F = 5.19$, $n = 167$, $p = 0.023$). Overall, states with higher consciousness levels (stimulation-induced arousal, wakefulness) showed increased deep cortical and thalamic activities, suggesting a role in the NCC.

Intracolumnar Interactions Showed Layer-Specific NCC

To measure state-related changes in thalamocortical and corticocortical communication, we calculated power and coherence using bipolar derivatized LFPs. We combined data across anesthetics, as effects were qualitatively similar (Figures S2H–S2O and S4A–S4H). We focus here on intracolumnar changes, particularly coherence within superficial layers, deep layers, and between superficial and deep layers of the same cortical area. Coherence changed markedly between wakefulness and anesthesia; anesthesia increased delta coherence (<4 Hz) and reduced alpha (8–15 Hz) and low gamma coherence (30–60 Hz; Figures 3A and 3B; Table S1 for complete

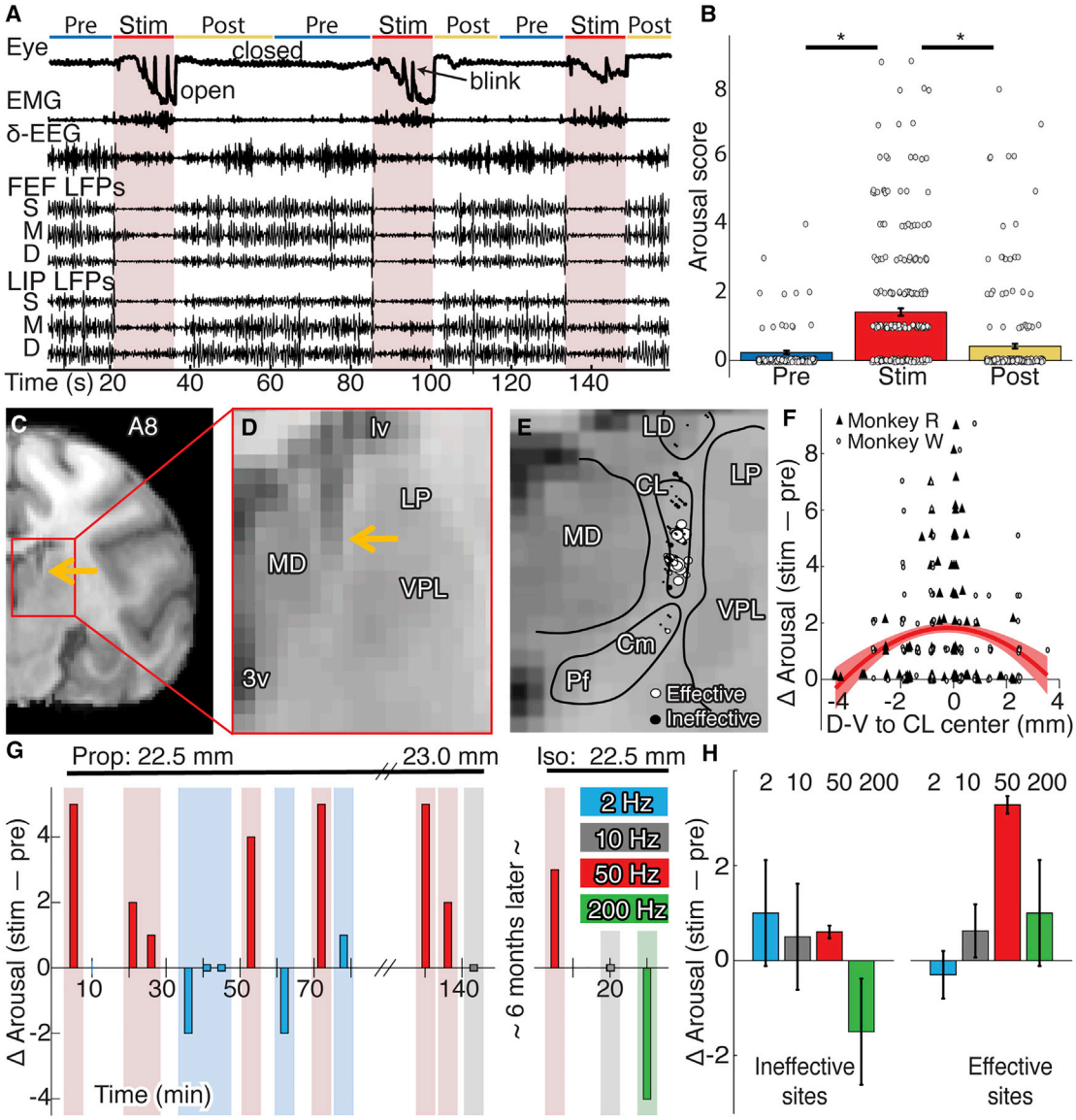

Figure 1. Gamma-Frequency CL Stimulation Increased Consciousness Level

(A) Example behavioral and neural recordings during 50-Hz stimulation (arousal score 5).

(B) Population mean arousal score (±SE) before, during, and after stimulations for both monkeys (circles show individual stimulation events).

(C) Coronal section of right hemisphere 8 mm anterior to interaural line (A8). The arrow shows the electrode.

(D) Magnified view of the thalamus.

(E) Stimulation sites in monkey R (n = 90) collapsed along the A-P axis. Circles represent the middle contact in the stimulation array; diameter scales with induced arousal.

(F) Stimulation-induced arousal change (score during stim–pre) as a function of the dorsal-ventral distance from CL center. Symbols show stimulation events by monkey; the red curve shows the quadratic fit (±SE).

(G) Example of stimulation series for different frequencies during propofol (left) and isoflurane (right) at the same site 22.5 mm ventral to the cortical surface.

(H) Population mean arousal change (±SE of point estimate) for different stimulation frequencies at effective and ineffective sites from both monkeys.

statistics). Wake-anesthesia differences were consistent between different layers of FEF and LIP (Figures 3C–3H) and qualitatively similar to differences between wakefulness and NREM sleep (Figure S2). Notably, coherence between superficial and deep layers of both cortical areas showed substantial decreases in all higher-frequency (>4 Hz) communication during anesthesia ($T \geq 10.05$, n = 8,725, $p < 1.0 \times 10^{-10}$; Figures 3E and 3F; Table S1), suggesting altered processing in cortical microcircuits.

Effective 50-Hz thalamic stimulation increased intracolumnar coherence differentially across frequency bands and layers (Figures 3K–3P; Table S1 for complete statistics). Coherence within superficial layers was increased for effective compared to ineffective stimulations at low gamma (Figures 3K and 3L),

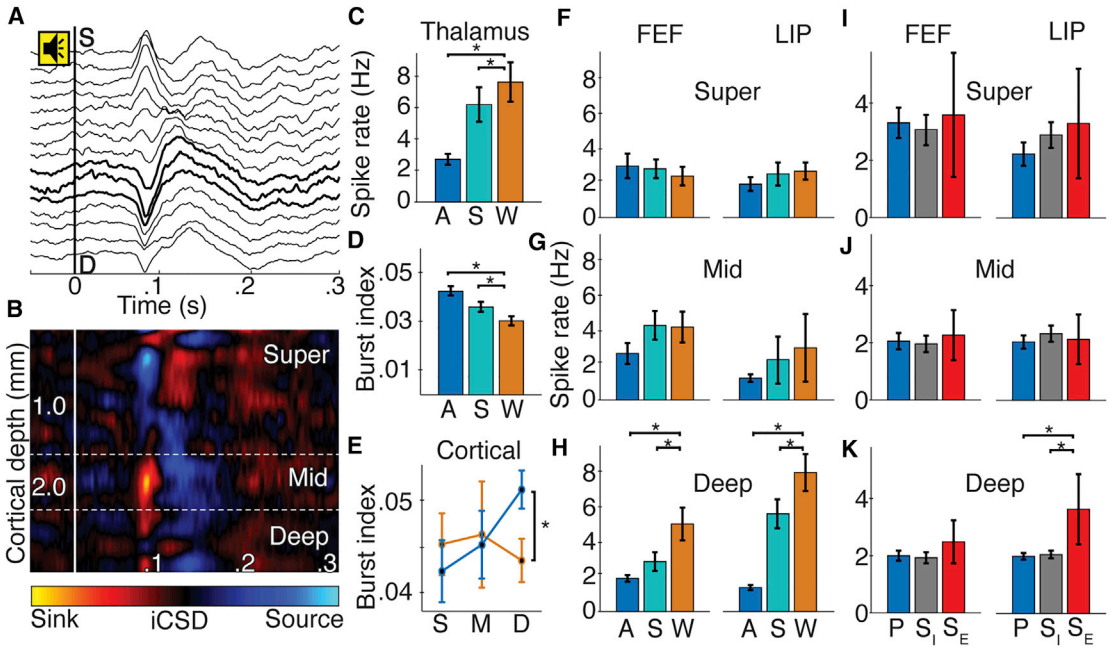

Figure 2. Consciousness Level Modulated Spike Rate and Timing in Deep Cortical Layers and CL

(A) Example of sound-aligned evoked potentials from linear multi-electrode array in FEF. Tone onset at 0 s. Bold lines show inverse CSD (iCSD)-defined middle layers.

(B) Sound-aligned iCSD corresponding to (A).

(C and D) Population CL spike rate (±SE) (C) and CL burst index (±SE) (D) for anesthesia (blue), sleep (teal), and wake (orange) states; *p < 0.05.

(E) Cortical (FEF and LIP) burst index (±SE) in superficial (S), middle (M), and deep (D) layers for wakefulness (orange) and anesthesia (blue).

(F–H) Superficial (F), middle (G), and deep (H) layer spike rates (±SE) in FEF and LIP across states.

(I–K) Superficial (I), middle (J), and deep (K) spike rates (±SE) in FEF and LIP during effective stimulation (S_E, red), ineffective stimulation (S_I, gray), and pre-stimulation (P, blue).

showing a significant interaction between stimulation and effectiveness ($T = 5.24$, $n = 2{,}387$, $p = 1.8 \times 10^{-6}$). Within deep layers (Figures 3O and 3P), similar interactions show that effective stimulations selectively increased coherence at theta (4–8 Hz, $T = 9.04$, $n = 2{,}183$, $p < 1.0 \times 10^{-10}$) and alpha ($T = 11.79$, $n = 2{,}183$, $p < 1.0 \times 10^{-10}$) frequencies. Important for intracolumnar processing, superficial and deep layers showed broadband coherence increases selective for effective stimulations at the same frequencies hindered by general anesthesia (bands > 4 Hz; $T \geq 4.83$, $n = 2{,}631$, $p \leq 1.3 \times 10^{-6}$; see Table S1). Note that power changes during thalamic stimulation did not correlate with coherence changes (Figures S3K–S3P; Table S2 for complete statistics), nor did power changes reflect behavioral arousal during stimulation.

Thalamocortical and Corticocortical Interactions Showed Pathway-Specific NCC

We next focus on anatomically motivated interactions across the frontoparietal cortex. We measured coherence between the origin and termination of putative feedforward (superficial LIP-superficial and middle FEF) and two feedback (deep FEF-superficial LIP or deep FEF-deep LIP) pathways (Markov et al., 2014; Mejias et al., 2016). We also examined state-dependent effects on thalamocortical coherence (CL-superficial or CL-deep cortical layers) (Molinari et al., 1994; Towns et al., 1990). Communication between cortical areas showed significant changes during general anesthesia (Figure 4A). Corticocortical coherence increased at delta and decreased at all higher frequencies across putative feedforward and feedback pathways ($|T| \geq 6.04$, $N \geq 4{,}030$, $p \leq 1.6 \times 10^{-9}$; Table S3 for complete statistics). We found qualitatively similar but smaller effects during NREM sleep (Figures S4C, S4F, and S4I) and for spike-field coherence (Figures S4J–S4L; Table S3 for complete statistics). Coherence between thalamus and either superficial or deep cortical layers decreased across all frequency bands during anesthesia (Figures 4I–4L; Table S4 for complete statistics). Thalamocortical spike-field coherence showed similar effects (Figures S4M–S4R; Table S4 for complete statistics). These results show that anesthesia decreases broadband thalamocortical and corticocortical coherence.

Thalamic stimulation isolated specific interactions between cortical areas important for consciousness (Figure 4E). Effective stimulations resulted in targeted restoration of frontoparietal coherence in putative feedforward and feedback pathways (Figures 4F–4H). Coherence between superficial layers of LIP and superficial and middle FEF substantially reduced at delta ($T = -4.05$, $n = 2{,}799$, $p = 8.6 \times 10^{-4}$), and increased at alpha ($T = 6.87$, $n = 2{,}799$, $p = 1.46 \times 10^{-10}$), low gamma ($T = 4.45$, $n = 2{,}799$, $p = 1.50 \times 10^{-4}$), and high gamma (60–90 Hz; $T = 3.03$, $n = 2{,}799$, $p = 0.027$), for effective more than ineffective stimulations, as shown by significant interactions (Figure 4F). There was also a significant interaction for coherence between deep layers of FEF and superficial LIP at alpha (Figure 4G; $T = 3.97$, $n = 1{,}617$, $p = 0.001$), showing

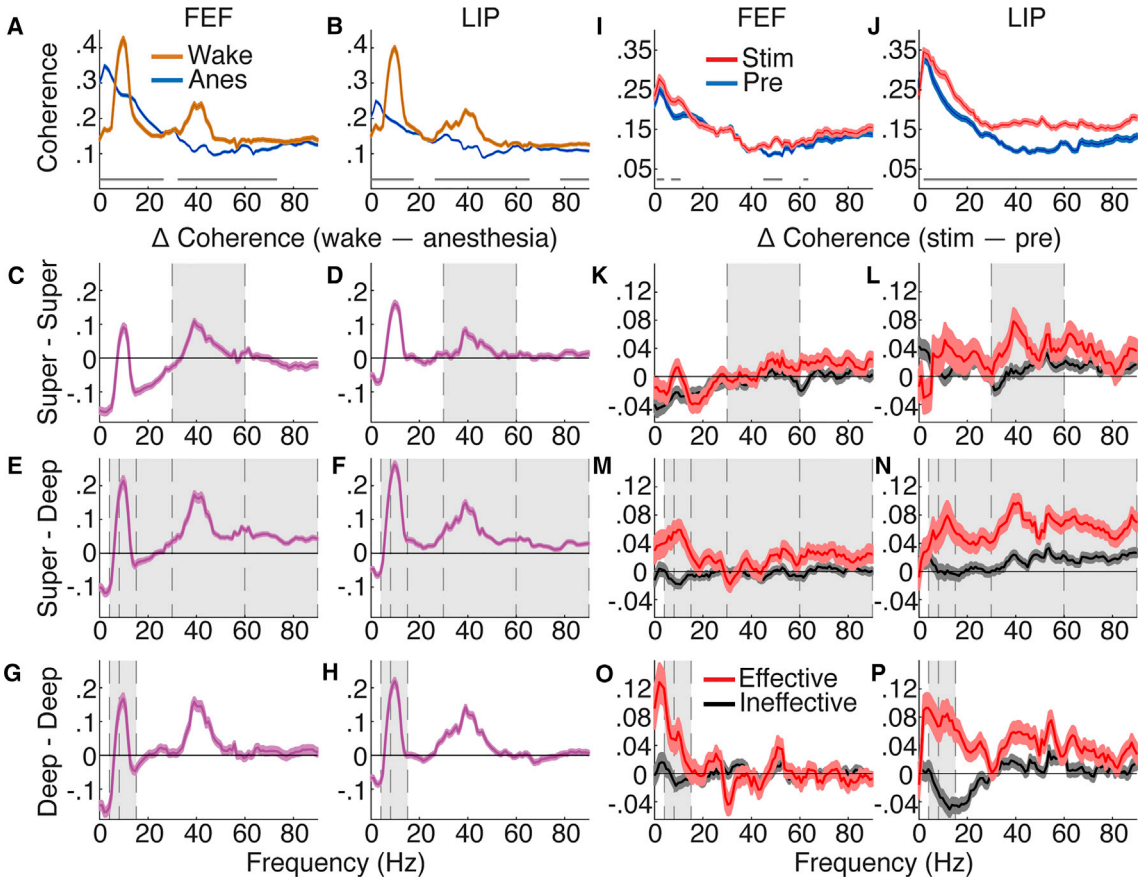

Figure 3. Intracolumnar Interactions Show Layer-Specific NCC

(A and B) Population FEF (A) and LIP (B) coherence with 95% confidence intervals for wakefulness and anesthesia. Average of all contact pairs across layers. The gray lines show significant differences between spectra (Holm's corrected t tests).

(C–H) Population coherence difference between wakefulness and anesthesia. Positive when wake > anesthesia. The error bars indicate 95% confidence intervals of t tests at each frequency. The gray shading shows effects consistent between state (wake versus anesthesia) and thalamic stimulation (effective versus ineffective in K–P) results. Average of all contact pairs for and between superficial (C) FEF and (D) LIP; superficial and deep (E) FEF and (F) LIP; and deep (G) FEF and (H) LIP.

(I and J) Population FEF (I) and LIP (J) coherence with 95% confidence intervals under anesthesia before and during effective stimulation. Average across all layers.

(K–P) Population coherence difference (stim–pre) with 95% confidence intervals for effective and ineffective stimulations. Positive when stim > pre. Average of all contact pairs for and between superficial (K) FEF and (L) LIP; superficial and deep (M) FEF and (N) LIP; and deep (O) FEF and (P) LIP.

substantial increases in alpha coherence specific to effective stimulations. While coherence between FEF and LIP deep cortical layers did generally increase with stimulation, no interactions were significant (Figure 4H; Table S3 for complete statistics). Overall, more-conscious states showed increased alpha and gamma coherence in feedforward pathways as well as alpha coherence in the feedback pathways originating in deep layers and terminating in superficial layers of the lower-order area.

DISCUSSION

Circuit-Level Mechanism for Consciousness and Anesthesia

Our results suggest that specific feedforward and feedback corticocortical path as well as intracolumnar and thalamocortical circuit dynamics contribute to the NCC (Figure 4M). We link consciousness to increased spiking activity in deep cortical layers and CL, which is consistent with cat and rodent studies of V1 (Livingstone and Hubel, 1981; Senzai et al., 2019) and CL (Glenn and Steriade, 1982) comparing wakefulness and NREM sleep. This spiking activity is likely sustained through reciprocal deep-layer cortex-CL connections, because reduced deep cortical layer and CL spiking coincided with reduced functional connectivity between CL and cortex, and CL stimulation increased deep cortical layer spiking.

The deep cortical layers are anatomically positioned to drive feedback to superficial layers in lower-order areas, and to influence feedforward pathways via interactions with superficial layers in the same cortical column. CL, with projections both to superficial and deep cortical layers, can modulate

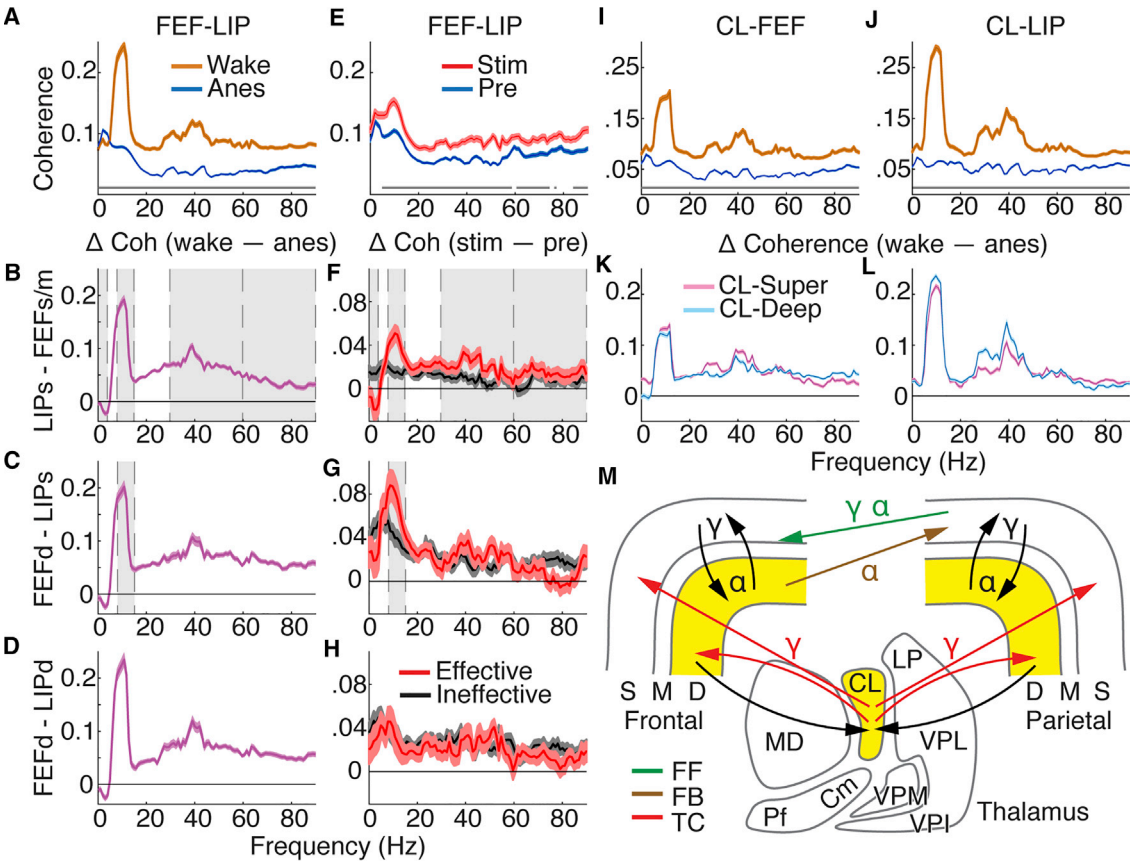

Figure 4. Thalamocortical and Corticocortical Interactions Show Pathway-Specific NCC

(A) Population coherence with 95% confidence intervals for all paired contacts between FEF and LIP during wakefulness and anesthesia. The gray lines show significant differences between spectra (Holm's corrected t tests).

(B–D) Population average coherence difference: wake–anesthesia. The error bars indicate 95% confidence intervals of t tests at each frequency. The gray shading shows effects consistent between state and thalamic stimulation (in F–H) results. (B) Superficial LIP and superficial and middle FEF; (C) deep FEF and superficial LIP; and (D) deep FEF and deep LIP.

(E) Population coherence between FEF and LIP with 95% confidence intervals for all paired contacts under anesthesia, before and during effective stimulation.

(F–H) Population average coherence difference, stim–pre, with 95% confidence intervals for effective and ineffective stimulations. (F) Superficial LIP and superficial and middle FEF; (G) deep FEF and superficial LIP; and (H) deep FEF and deep LIP.

(I and J) Population thalamocortical coherence with 95% confidence intervals for wake and anesthesia across all paired CL-FEF (I) and CL-LIP (J) contacts.

(K and L) Population average thalamocortical coherence difference, wake–anesthesia, with 95% confidence intervals of t tests. CL-superficial and CL-deep layers for (K) FEF and (L) LIP.

(M) Schematic showing pathways and predominant frequencies contributing to NCC. Yellow shading where spiking changes with consciousness level. FF, feedforward; FB, feedback; TC, thalamocortical.

intracolumnar and cross-area interactions (Purpura and Schiff, 1997). These interactions operated at alpha and gamma frequencies during consciousness, whereas general anesthesia and sleep reduced activity in deep cortical layers and CL, thus reducing alpha and gamma frequency communication within and between cortical areas. Reactivation of this CL-deep cortical layer loop with gamma-frequency stimulation reinstated wake-like cortical dynamics and increased the consciousness level, overcoming two separate anesthetics with different molecular targets. Overall, our study provides empirical evidence for a circuit-level mechanism of consciousness with special emphasis on the reciprocal interaction between CL and deep cortical layers, which may serve as a common target of anesthetic drugs, particularly those with actions on the GABA-A receptor.

Specificity of Effective Thalamic Stimulation Points to Minimal and Sufficient Mechanisms for Consciousness

Our results suggest that CL has a special role to play in consciousness, as stimulations were most effective when centered on CL as opposed to neighboring thalamic areas, such as the mediodorsal (MD) and centromedian (CM) nuclei. Thus, the unique properties of CL have important implications for consciousness. CL projects to superficial and deep layers of the frontal and the parietal cortex (Kaufman and Rosenquist, 1985; Purpura and Schiff, 1997; Towns et al., 1990).

This projection pattern differs substantially from the MD, which largely projects to the prefrontal cortex and has different laminar distribution (Erickson and Lewis, 2004; Giguere and Goldman-Rakic, 1988; Ray and Price, 1993). While cholinergic stimulation of frontal cortex has proven sufficient for behavioral arousal in rodents (Pal et al., 2018), prefrontal stimulation via the MD proved less effective in our macaques. This suggests that prefrontal activation alone, via the MD, is insufficient for consciousness. CL also has a prominent projection to the striatum, which could contribute to consciousness. However, the CM, with a stronger projection to the striatum but limited cortical projections (Smith et al., 2004), was less effective than CL stimulation at inducing consciousness. This suggests that activation of the direct thalamo-striatal path is insufficient for consciousness. Our results further support coordinated activity across the CL and the frontoparietal cortex as NCC.

Validating NCC with Multiple Conscious and Unconscious States

Changes in consciousness coincide with state changes across sleep and wake cycles, traumatic brain injury, or exposure to a wide range of anesthetic agents with different molecular targets. As such, it can be difficult to distinguish NCC from neural effects specific to one of these states, such as effects of attention, trauma, or a particular pharmacological agent. In this study, we show NCC in a thalamocortical system that are (1) similarly perturbed in natural (sleep) and two induced states of unconsciousness with different pharmacological agents (isoflurane or propofol), and (2) validated in two states of consciousness, normal wakefulness, and stimulation-induced arousal during continuous anesthetic administration (Figures 3 and 4, gray shading). This shows that our results are neither drug specific nor purely reflecting an unnatural state of consciousness. Rather, our results show consistent NCC and point to a common circuit-level target of general anesthetics.

Beyond Delta: Path-Specific Indicators of Level of Consciousness

Since the early studies of consciousness, electroencephalogram (EEG) delta activity has been considered critical for sleep staging and monitoring depth of anesthesia. Our results show that delta activity, while prevalent in unconscious states (isoflurane, propofol, and sleep), differs between the frontal and the parietal cortex, as well as across cortical layers, and is not itself a predictor of behavioral arousal (Figures S3A–S3H). Furthermore, we found that while delta coherence was anticorrelated with consciousness in feedforward pathways, possibly demonstrating a mechanism for disconnection, there was no such relation for feedback pathways (Figures 4F–4H). If delta oscillations do facilitate corticocortical disconnection, our findings suggest that they do so in a pathway-specific manner, in which feedforward processes are readily disrupted by the increased prevalence of delta activity relative to feedback. Thus, delta oscillations may play a larger role in disconnecting the brain from the external sensory environment than in preventing internal and top-down generated experiences.

Long-Range Frontoparietal Interaction Contributes to Consciousness, Not Just Report

Frontal cortical activity, in studies of consciousness requiring behavioral reports, may reflect the report rather than the level of consciousness (Tsuchiya et al., 2015). Our study did not require report (although it cannot be ruled out completely that observed activity reflects an underlying process related to reporting). Furthermore, to rule out sensorimotor differences between different states of consciousness, we performed recordings in a quiet, dark room and only analyzed data from epochs when the monkey's eyes were stable, thereby controlling for sensory stimulation and eye movements. Under these conditions, we found frontoparietal interaction featured during wakefulness and stimulation-induced arousal, appearing rapidly after the onset of thalamic stimulation and generally dissipating just as quickly after stimulation ended in anesthetized monkeys. This suggests that frontoparietal communication may not simply be related to report, but rather contributes to the conscious experience. Because feedback projections to distant cortical areas preferentially terminate in superficial layers (whereas feedback to adjacent areas preferentially terminate in deep layers) (Markov et al., 2014), our finding that feedback to superficial layers correlated with the level of consciousness may suggest that long-range feedback projections are vital for consciousness.

Implications for Clinical Interventions in Disorders of Consciousness

Interventions using clinical deep brain stimulation (DBS) electrodes in humans (Schiff et al., 2007) and monkeys (Baker et al., 2016) and bipolar stimulating electrodes in rodents (Mair and Hembrook, 2008; Shirvalkar et al., 2006) have shown arousal modulation with stimulation frequencies between 100 and 200 Hz. In comparison, using a linear multi-electrode array with a small electrode contact size, we found that CL stimulation most effectively induced arousal at 50 Hz (cf. with 2, 10, and 200 Hz). CL is an elongated nucleus along the dorsal-ventral axis, ~3–4 mm in extent in macaques. By using linear multi-electrode arrays (simultaneously stimulating 16 contacts, with 200-μm inter-contact spacing), we were able to stimulate across the dorsal-ventral extent of CL at small, regularly spaced intervals in a relatively precise way. This configuration led to the greatest behavioral effects (Figures 1F and S1D–S1F), demonstrating clear spatial specificity. While our study did not test the full range of clinically relevant stimulation frequencies, it is interesting to note that 50-Hz stimulation in our study, and the more spatially refined 40- and 100-Hz optogenetic stimulation in a rat sleep study (Liu et al., 2015), modulated arousal. These frequencies match the activity patterns of the subset of CL neurons with a high firing rate during wakefulness, reported in Figures S2E and S2F and previous work (Glenn and Steriade, 1982; Steriade et al., 1993). Mimicking the wakeful firing rate of these neurons during anesthetic administration may partially explain the increased efficacy of gamma stimulation in our data. In light of these results, it may be possible to optimize clinical DBS to better reflect the desired neural dynamics of affected thalamocortical circuits to help alleviate disorders of consciousness.

STAR★METHODS

Detailed methods are provided in the online version of this paper and include the following:

- KEY RESOURCES TABLE
- LEAD CONTACT AND MATERIALS AVAILABILITY
- EXPERIMENTAL MODEL AND SUBJECT DETAILS
- METHOD DETAILS
  - Neuroimaging
  - Surgery
  - Behavioral tasks and sensory stimuli
  - Arousal scoring
  - Electrophysiological recording and stimulation
  - Electrode array localization
  - Anesthesia experiments
  - Awake experiments
  - Sleep
  - Neural data preprocessing
  - Spike rate
  - Spike timing
  - Current source density (CSD)
  - Power
  - Coherence
- QUANTIFICATION AND STATISTICAL ANALYSIS
  - General approach
  - Stimulation effects
  - Spike rate effects
  - Bursting effects
  - Power and coherence effects
- DATA AND CODE AVAILABILITY

SUPPLEMENTAL INFORMATION

Supplemental Information can be found online at https://doi.org/10.1016/j.neuron.2020.01.005.

ACKNOWLEDGMENTS

We thank M.I. Banks, C.W. Berridge, R.A. Pearce, R.D. Sanders, B.M. Krause, and C. Murphy for useful comments on the manuscript. This work was supported by NIH grants R01MH110311 and P51OD011106, BSF grant 201732, and a WNPRC pilot grant.

AUTHOR CONTRIBUTIONS

M.J.R., J.M.P., N.A.K., S.M., A.R., and Y.B.S. performed the research; M.J.R., S.A., G.L.D., M.A., and Y.B.S. analyzed the data; M.J.R., A.R., and Y.B.S. wrote the paper; M.J.R., J.M.P., N.A.K., S.M., S.A., G.L.D., M.A., A.R., and Y.B.S. edited the paper.

DECLARATION OF INTERESTS

A.R. is a consultant for and receives funding from Medtronic. The other authors declare no competing interests.

Received: November 19, 2019
Revised: December 26, 2019
Accepted: January 7, 2020
Published: February 12, 2020

REFERENCES

Baker, R., Gent, T.C., Yang, Q., Parker, S., Vyssotski, A.L., Wisden, W., Brickley, S.G., and Franks, N.P. (2014). Altered activity in the central medial thalamus precedes changes in the neocortex during transitions into both sleep and propofol anesthesia. J. Neurosci. *34*, 13326–13335.

Baker, J.L., Ryou, J.W., Wei, X.F., Butson, C.R., Schiff, N.D., and Purpura, K.P. (2016). Robust modulation of arousal regulation, performance, and frontostriatal activity through central thalamic deep brain stimulation in healthy nonhuman primates. J. Neurophysiol. *116*, 2383–2404.

Bokil, H., Purpura, K., Schoffelen, J.M., Thomson, D., and Mitra, P. (2007). Comparing spectra and coherences for groups of unequal size. J. Neurosci. Methods *159*, 337–345.

Bokil, H., Andrews, P., Kulkarni, J.E., Mehta, S., and Mitra, P.P. (2010). Chronux: a platform for analyzing neural signals. J. Neurosci. Methods *192*, 146–151.

Bollimunta, A., Chen, Y., Schroeder, C.E., and Ding, M. (2008). Neuronal mechanisms of cortical alpha oscillations in awake-behaving macaques. J. Neurosci. *28*, 9976–9988.

Boly, M., Garrido, M.I., Gosseries, O., Bruno, M.A., Boveroux, P., Schnakers, C., Massimini, M., Litvak, V., Laureys, S., and Friston, K. (2011). Preserved feedforward but impaired top-down processes in the vegetative state. Science *332*, 858–862.

Bruce, C.J., Goldberg, M.E., Bushnell, M.C., and Stanton, G.B. (1985). Primate frontal eye fields. II. Physiological and anatomical correlates of electrically evoked eye movements. J. Neurophysiol. *54*, 714–734.

Caruso, V.C., Pages, D.S., Sommer, M.A., and Groh, J.M. (2016). Similar prevalence and magnitude of auditory-evoked and visually evoked activity in the frontal eye fields: implications for multisensory motor control. J. Neurophysiol. *115*, 3162–3173.

Chen, X., Zirnsak, M., and Moore, T. (2018). Dissonant Representations of Visual Space in Prefrontal Cortex during Eye Movements. Cell Rep. *22*, 2039–2052.

Cohen, Y.E., Russ, B.E., and Gifford, G.W., 3rd (2005). Auditory processing in the posterior parietal cortex. Behav. Cogn. Neurosci. Rev. *4*, 218–231.

Contreras, D., Destexhe, A., Sejnowski, T.J., and Steriade, M. (1997). Spatiotemporal patterns of spindle oscillations in cortex and thalamus. J. Neurosci. *17*, 1179–1196.

Dehaene, S., and Changeux, J.P. (2011). Experimental and theoretical approaches to conscious processing. Neuron *70*, 200–227.

Erez, Y., Tischler, H., Moran, A., and Bar-Gad, I. (2010). Generalized framework for stimulus artifact removal. J. Neurosci. Methods *191*, 45–59.

Erickson, S.L., and Lewis, D.A. (2004). Cortical connections of the lateral mediodorsal thalamus in cynomolgus monkeys. J. Comp. Neurol. *473*, 107–127.

Friston, K. (2010). The free-energy principle: a unified brain theory? Nat. Rev. Neurosci. *11*, 127–138.

Funk, C.M., Honjoh, S., Rodriguez, A.V., Cirelli, C., and Tononi, G. (2016). Local Slow Waves in Superficial Layers of Primary Cortical Areas during REM Sleep. Curr. Biol. *26*, 396–403.

Gifford, G.W., 3rd, and Cohen, Y.E. (2005). Spatial and non-spatial auditory processing in the lateral intraparietal area. Exp. Brain Res. *162*, 509–512.

Giguere, M., and Goldman-Rakic, P.S. (1988). Mediodorsal nucleus: areal, laminar, and tangential distribution of afferents and efferents in the frontal lobe of rhesus monkeys. J. Comp. Neurol. *277*, 195–213.

Glenn, L.L., and Steriade, M. (1982). Discharge rate and excitability of cortically projecting intralaminar thalamic neurons during waking and sleep states. J. Neurosci. *2*, 1387–1404.

Grunewald, A., Linden, J.F., and Andersen, R.A. (1999). Responses to auditory stimuli in macaque lateral intraparietal area. I. Effects of training. J. Neurophysiol. *82*, 330–342.

Haegens, S., Barczak, A., Musacchia, G., Lipton, M.L., Mehta, A.D., Lakatos, P., and Schroeder, C.E. (2015). Laminar Profile and Physiology of the α Rhythm

in Primary Visual, Auditory, and Somatosensory Regions of Neocortex. J. Neurosci. *35*, 14341–14352.

Jenkinson, M., Beckmann, C.F., Behrens, T.E., Woolrich, M.W., and Smith, S.M. (2012). Fsl. Neuroimage *62*, 782–790.

Jones, E.G. (2009). Synchrony in the interconnected circuitry of the thalamus and cerebral cortex. Ann. NY Acad. Sci. *1157*, 10–23.

Katzner, S., Nauhaus, I., Benucci, A., Bonin, V., Ringach, D.L., and Carandini, M. (2009). Local origin of field potentials in visual cortex. Neuron *61*, 35–41.

Kaufman, E.F., and Rosenquist, A.C. (1985). Efferent projections of the thalamic intralaminar nuclei in the cat. Brain Res. *335*, 257–279.

Lacey, C.J., Bolam, J.P., and Magill, P.J. (2007). Novel and distinct operational principles of intralaminar thalamic neurons and their striatal projections. J. Neurosci. *27*, 4374–4384.

Lamme, V.A. (2006). Towards a true neural stance on consciousness. Trends Cogn. Sci. *10*, 494–501.

Lee, U., Kim, S., Noh, G.J., Choi, B.M., Hwang, E., and Mashour, G.A. (2009). The directionality and functional organization of frontoparietal connectivity during consciousness and anesthesia in humans. Conscious. Cogn. *18*, 1069–1078.

Lee, U., Ku, S., Noh, G., Baek, S., Choi, B., and Mashour, G.A. (2013). Disruption of frontal-parietal communication by ketamine, propofol, and sevoflurane. Anesthesiology *118*, 1264–1275.

Linden, J.F., Grunewald, A., and Andersen, R.A. (1999). Responses to auditory stimuli in macaque lateral intraparietal area. II. Behavioral modulation. J. Neurophysiol. *82*, 343–358.

Liu, J., Lee, H.J., Weitz, A.J., Fang, Z., Lin, P., Choy, M., Fisher, R., Pinskiy, V., Tolpygo, A., Mitra, P., et al. (2015). Frequency-selective control of cortical and subcortical networks by central thalamus. eLife *4*, e09215.

Livingstone, M.S., and Hubel, D.H. (1981). Effects of sleep and arousal on the processing of visual information in the cat. Nature *291*, 554–561.

Llinás, R., Ribary, U., Contreras, D., and Pedroarena, C. (1998). The neuronal basis for consciousness. Philos. Trans. R. Soc. Lond. B Biol. Sci. *353*, 1841–1849.

Maimon, G., and Assad, J.A. (2009). Beyond Poisson: increased spike-time regularity across primate parietal cortex. Neuron *62*, 426–440.

Mair, R.G., and Hembrook, J.R. (2008). Memory enhancement with event-related stimulation of the rostral intralaminar thalamic nuclei. J. Neurosci. *28*, 14293–14300.

Maksimow, A., Silfverhuth, M., Långsjö, J., Kaskinoro, K., Georgiadis, S., Jääskeläinen, S., and Scheinin, H. (2014). Directional connectivity between frontal and posterior brain regions is altered with increasing concentrations of propofol. PLoS One *9*, e113616.

Markov, N.T., Vezoli, J., Chameau, P., Falchier, A., Quilodran, R., Huissoud, C., Lamy, C., Misery, P., Giroud, P., Ullman, S., et al. (2014). Anatomy of hierarchy: feedforward and feedback pathways in macaque visual cortex. J. Comp. Neurol. *522*, 225–259.

Mejias, J.F., Murray, J.D., Kennedy, H., and Wang, X.J. (2016). Feedforward and feedback frequency-dependent interactions in a large-scale laminar network of the primate cortex. Sci. Adv. *2*, e1601335.

Mitra, P., and Bokil, H. (2007). Observed Brain Dynamics (Oxford University Press).

Molinari, M., Leggio, M.G., Dell'Anna, M.E., Giannetti, S., and Macchi, G. (1994). Chemical compartmentation and relationships between calcium-binding protein immunoreactivity and layer-specific cortical caudate-projecting cells in the anterior intralaminar nuclei of the cat. Eur. J. Neurosci. *6*, 299–312.

Oizumi, M., Albantakis, L., and Tononi, G. (2014). From the phenomenology to the mechanisms of consciousness: Integrated Information Theory 3.0. PLoS Comput. Biol. *10*, e1003588.

Pal, D., Dean, J.G., Liu, T., Li, D., Watson, C.J., Hudetz, A.G., and Mashour, G.A. (2018). Differential Role of Prefrontal and Parietal Cortices in Controlling Level of Consciousness. Curr. Biol. *28*, 2145–2152.e5.

Pettersen, K.H., Devor, A., Ulbert, I., Dale, A.M., and Einevoll, G.T. (2006). Current-source density estimation based on inversion of electrostatic forward solution: effects of finite extent of neuronal activity and conductivity discontinuities. J. Neurosci. Methods *154*, 116–133.

Pigarev, I.N., Saalmann, Y.B., and Vidyasagar, T.R. (2009). A minimally invasive and reversible system for chronic recordings from multiple brain sites in macaque monkeys. J. Neurosci. Methods *181*, 151–158.

Purpura, K., and Schiff, N.D. (1997). The Thalamic Intralaminar Nuclei: A Role in Visual Awareness. Neuroscientist *3*, 8.

Ray, J.P., and Price, J.L. (1993). The organization of projections from the mediodorsal nucleus of the thalamus to orbital and medial prefrontal cortex in macaque monkeys. J. Comp. Neurol. *337*, 1–31.

Raz, A., Grady, S.M., Krause, B.M., Uhlrich, D.J., Manning, K.A., and Banks, M.I. (2014). Preferential effect of isoflurane on top-down vs. bottom-up pathways in sensory cortex. Front. Syst. Neurosci. *8*, 191.

Romanski, L.M., Tian, B., Fritz, J., Mishkin, M., Goldman-Rakic, P.S., and Rauschecker, J.P. (1999). Dual streams of auditory afferents target multiple domains in the primate prefrontal cortex. Nat. Neurosci. *2*, 1131–1136.

Saalmann, Y.B., Pigarev, I.N., and Vidyasagar, T.R. (2007). Neural mechanisms of visual attention: how top-down feedback highlights relevant locations. Science *316*, 1612–1615.

Saalmann, Y.B., Pinsk, M.A., Wang, L., Li, X., and Kastner, S. (2012). The pulvinar regulates information transmission between cortical areas based on attention demands. Science *337*, 753–756.

Saleem, K.S., and Logothetis, N.K. (2007). A Combined MRI and Histology Atlas of the Rhesus Monkey Brain in Stereotaxic Coordinates (Academic Press).

Sanders, R.D., Banks, M.I., Darracq, M., Moran, R., Sleigh, J., Gosseries, O., Bonhomme, V., Brichant, J.F., Rosanova, M., Raz, A., et al. (2018). Propofol-induced unresponsiveness is associated with impaired feedforward connectivity in cortical hierarchy. Br. J. Anaesth. *121*, 1084–1096.

Schall, J.D., Morel, A., King, D.J., and Bullier, J. (1995). Topography of visual cortex connections with frontal eye field in macaque: convergence and segregation of processing streams. J. Neurosci. *15*, 4464–4487.

Schiff, N.D. (2008). Central thalamic contributions to arousal regulation and neurological disorders of consciousness. Ann. N Y Acad. Sci. *1129*, 105–118.

Schiff, N.D., Giacino, J.T., Kalmar, K., Victor, J.D., Baker, K., Gerber, M., Fritz, B., Eisenberg, B., Biondi, T., O'Connor, J., et al. (2007). Behavioural improvements with thalamic stimulation after severe traumatic brain injury. Nature *448*, 600–603.

Schmitt, L.I., Wimmer, R.D., Nakajima, M., Happ, M., Mofakham, S., and Halassa, M.M. (2017). Thalamic amplification of cortical connectivity sustains attentional control. Nature *545*, 219–223.

Schroeder, C.E., Mehta, A.D., and Givre, S.J. (1998). A spatiotemporal profile of visual system activation revealed by current source density analysis in the awake macaque. Cereb. Cortex *8*, 575–592.

Sellers, K.K., Bennett, D.V., Hutt, A., and Fröhlich, F. (2013). Anesthesia differentially modulates spontaneous network dynamics by cortical area and layer. J. Neurophysiol. *110*, 2739–2751.

Senzai, Y., Fernandez-Ruiz, A., and Buzsaki, G. (2019). Layer-Specific Physiological Features and Interlaminar Interactions in the Primary Visual Cortex of the Mouse. Neuron *101*, 500–513.e5.

Shirvalkar, P., Seth, M., Schiff, N.D., and Herrera, D.G. (2006). Cognitive enhancement with central thalamic electrical stimulation. Proc. Natl. Acad. Sci. USA *103*, 17007–17012.

Smith, Y., Raju, D.V., Pare, J.F., and Sidibe, M. (2004). The thalamostriatal system: a highly specific network of the basal ganglia circuitry. Trends Neurosci. *27*, 520–527.

Steriade, M., Curró Dossi, R., and Contreras, D. (1993). Electrophysiological properties of intralaminar thalamocortical cells discharging rhythmic (approximately 40 HZ) spike-bursts at approximately 1000 HZ during waking and rapid eye movement sleep. Neuroscience *56*, 1–9.

Theyel, B.B., Llano, D.A., and Sherman, S.M. (2010). The corticothalamocortical circuit drives higher-order cortex in the mouse. Nat. Neurosci. *13*, 84–88.

Towns, L.C., Tigges, J., and Tigges, M. (1990). Termination of thalamic intralaminar nuclei afferents in visual cortex of squirrel monkey. Vis. Neurosci. *5*, 151–154.

Trongnetrpunya, A., Nandi, B., Kang, D., Kocsis, B., Schroeder, C.E., and Ding, M. (2016). Assessing Granger Causality in Electrophysiological Data: Removing the Adverse Effects of Common Signals via Bipolar Derivations. Front. Syst. Neurosci. *9*, 189.

Tsuchiya, N., Wilke, M., Frässle, S., and Lamme, V.A.F. (2015). No-Report Paradigms: Extracting the True Neural Correlates of Consciousness. Trends Cogn. Sci. *19*, 757–770.

Uhrig, L., Sitt, J.D., Jacob, A., Tasserie, J., Barttfeld, P., Dupont, M., Dehaene, S., and Jarraya, B. (2018). Resting-state Dynamics as a Cortical Signature of Anesthesia in Monkeys. Anesthesiology *129*, 942–958.

van Vugt, B., Dagnino, B., Vartak, D., Safaai, H., Panzeri, S., Dehaene, S., and Roelfsema, P.R. (2018). The threshold for conscious report: signal loss and response bias in visual and frontal cortex. Science *360*, 537–542.

Wardak, C., Olivier, E., and Duhamel, J.R. (2002). Saccadic target selection deficits after lateral intraparietal area inactivation in monkeys. J. Neurosci. *22*, 9877–9884.

Wardak, C., Ibos, G., Duhamel, J.R., and Olivier, E. (2006). Contribution of the monkey frontal eye field to covert visual attention. J. Neurosci. *26*, 4228–4235.

Womelsdorf, T., Ardid, S., Everling, S., and Valiante, T.A. (2014). Burst firing synchronizes prefrontal and anterior cingulate cortex during attentional control. Curr. Biol. *24*, 2613–2621.

STAR★METHODS

KEY RESOURCES TABLE

REAGENT or RESOURCE	SOURCE	IDENTIFIER
Chemicals, Peptides, and Recombinant Proteins		
Isoflurane, USP	Piramal Enterprises Limited	NDC 66794-013-25
PropoFlo 28 (Propofol)	Zoetis Inc.	NDC 54771-4944-1
KETAVED (KETAMINE HCL 100MG)	Vedco Inc.	NDC 50989-996-06
Experimental Models: Organisms/Strains		
Monkeys (Macaca mulatta)	Wisconsin National Primate Research Center (WNPRC)	https://www.primate.wisc.edu/
Software and Algorithms		
OmniPlex Server v 1.14.1	Plexon	https://plexon.com/products/omniplex-software/
PlexContron v 1.14.1	Plexon	https://plexon.com/products/omniplex-software/
Plexon Stim-2 v 2.3.0.0	Plexon	https://plexon.com/products/plexstim-electrical-stimulator-2-system/
Presentation v 19.0	Neurobehavioral Systems	https://www.neurobs.com/
Logitech Webcam Software v 2.51	Logitech	https://support.logi.com/hc/en-us/articles/360024691274–Downloads-Webcam-C260
Fsl v 1.6	Oxford University Innovation	https://fsl.fmrib.ox.ac.uk/fsldownloads_registration
Fsleyes v 0.22.6	Oxford University Innovation	https://fsl.fmrib.ox.ac.uk/fsldownloads_registration
XQuartz v 2.7.11	X.Org Foundation	https://www.xquartz.org/
Offline Sorter v4	Plexon	https://plexon.com/products/offline-sorter/
MATLAB R2015b	MathWorks	https://www.mathworks.com/products.html?s_tid=gn_ps
Chronux v 2.11	chronux	http://chronux.org/
SARGE toolbox v 1.5.4	IBG Lab	https://www.ibglab.org/sarge
CSDplotter v 0.1.1	Klas Pettersen (klas.pettersen@umb.no.)	https://github.com/espenhgn/CSDplotter
R v 3.2.2	R Foundation for Statistical Computing	https://www.r-project.org/
RStudio v 1.1.463	R Studio	https://rstudio.com/
Movavi Video Converter v 7.3.0	Movavi	https://www.movavi.com/videoconvertermac/?device=c&gclid=Cj0KCQiAtrnuBRDXARIsABiN-7BytoiOxcGD8lyR3Fvs1MGc3zWwA0UisQaA1DdujFHHS_q1fbZk6WwaAlnlEALw_wcB
Elmedia video player v 7.6	Elmedia Player	https://www.elmedia-video-player.com/
Other		
Macaque Stimulated Arousal Index	This paper	STAR Methods, Email (mredinbaugh@wisc.edu)

LEAD CONTACT AND MATERIALS AVAILABILITY

This study did not generate new unique reagents. Further information and requests regarding resources, equipment, and experimental methods should be directed to, and will be fulfilled by, the Lead Contact, Yuri B. Saalmann (saalmann@wisc.edu).

EXPERIMENTAL MODEL AND SUBJECT DETAILS

We acquired data from two male monkeys (*Macaca mulatta,* 4.3-5.5 years old, 7.63-10.30 kg body weight). Animal daily needs maintained by experimenters and husbandry staff at the Wisconsin National Primate Research Center (WNPRC), where animals were housed. Animal health was monitored by veterinarians at the WNPRC. The University of Wisconsin-Madison Institutional Animal Care and Use Committee approved all procedures, which conformed to the National Institutes of Health Guide for the Care and Use of Laboratory Animals.

METHOD DETAILS

Neuroimaging

We performed structural imaging on anesthetized monkeys using the GE MR750 3T scanner (GE Healthcare, Waukesha WI). At the start of each scan session, we pre-medicated the monkey with ketamine (up to 20 mg/kg body weight) and atropine sulfate (0.03-0.06 mg/kg), prior to intubation. We then administered isoflurane (1%–3% on ~1 L/min O_2 flow) to the monkey, with a semi-open breathing circuit and spontaneous respiration, to maintain general anesthesia for the duration of the session. We monitored the monkey's vital signs (expired carbon dioxide, respiration rate, oxygen saturation, pulse rate, temperature) using an MR-compatible pulse oximeter and rectal thermometer.

We acquired a high-resolution structural brain image prior to the implant surgery, to delineate thalamocortical regions of interest (ROIs), and, after craniotomy, additional scans of electrodes *in situ* to confirm electrode positioning. For these three dimensional T1-weighted structural images, we used an inversion-recovery prepared gradient echo sequence with the following parameters: FOV = 128 mm^2; matrix = 256 × 256; no. of slices = 166; 0.5 mm isotropic; TR = 9.68 ms; TE = 4.192 ms; flip angle = 12°; inversion time (TI) = 450 ms). To generate the high-quality structural image, we collected 6-10 T1-weighted structural images and calculated the average image for each monkey using the FMRIB Software Library (FSL) (Jenkinson et al., 2012). To localize electrodes, we averaged two structural images of electrodes *in situ*.

Surgery

We induced anesthesia with ketamine (up to 20 mg/kg body weight, i.m.) and maintained general anesthesia during aseptic surgical procedures with isoflurane (1%–2%). We used 12 ceramic skull screws and dental acrylic to affix head implants on monkeys. We drilled 2.5 mm craniotomies in the frontal and parietal bones within a customized plastic recording chamber, providing access to our three thalamocortical ROIs in the right hemisphere: frontal eye field (FEF), lateral intraparietal area (LIP), and central lateral thalamic nucleus (CL). We derived craniotomy coordinates from the high-quality T1-weighted structural images acquired prior to the surgery. We fitted each craniotomy with a conical plastic guide tube filled with bone wax (guide tube prefabricated using model of skull based on T1-weighted structural images) (Pigarev et al., 2009; Saalmann et al., 2007, 2012) through which linear electrode arrays traversed. We also inserted two titanium skull screws within the recording chamber, one from which to record the EEG and one to serve as a reference. The head implant included a head post and, on the implant left and right sides, four hollow slots (two on each side) into which rods fitted, allowing head immobilization during electrophysiological recordings.

Behavioral tasks and sensory stimuli

To compare electrophysiological data between different states of consciousness, we needed to acquire data under similar behavioral and sensory conditions for awake and anesthetized monkeys. Thus, we acquired electrophysiological data from both awake and anesthetized monkeys during a passive auditory oddball paradigm as well as during "resting state" (in which no sensory stimuli were presented). The passive auditory oddball paradigm was useful because it does not require a behavioral response, does not require open eyes, and auditory stimuli have been shown to elicit neuronal responses from FEF (Caruso et al., 2016; Romanski et al., 1999; Schall et al., 1995) and LIP (Cohen et al., 2005; Gifford and Cohen, 2005; Grunewald et al., 1999; Linden et al., 1999), allowing sound-aligned current source density analyses. Additionally, as controls in the awake monkeys, we acquired electrophysiology data during a fixation task, and during the passive auditory oddball paradigm while the monkey maintained fixation (oddball paradigm run concurrently with fixation task; see "Awake Experiments" section). All electrophysiological recordings occurred in a quiet, dark room.

In the passive auditory oddball paradigm, the sequence of auditory tones (200 ms duration, with 800 ± 100 ms jitter between each tone) comprised 80% standard tones (0.9 kHz frequency) and 20% deviant/oddball tones (1 kHz frequency). At least the first four stimuli of a sequence (3 min duration for anesthesia; 6 min duration for wake) were standard tones, and two sequential tones could not be deviant stimuli, otherwise the tone order was pseudorandom within the constraint of the overall 80/20 standard-to-deviant ratio. We presented tones using two speakers placed 35 cm from each ear under anesthesia and 80 cm from each ear during wakefulness (sound level at each ear was about 75 dB SPL for both states).

In the fixation task, the monkey needed to fixate a central fixation point (dim gray circle of diameter 0.42 degrees of visual angle on black background) on the monitor screen located 57 cm away. The monkey received a small volume (0.18-0.22 mL) of juice every 2.2-3.5 s while maintaining fixation within a 3 × 3 degree of visual angle window, centered on the fixation point. When the monkey's gaze left the fixation window, he would typically re-establish central fixation quickly, to again receive juice every 2.2-3.5 s while fixating. To encourage long fixations, we doubled the juice volume if fixation persisted beyond 10 s. We only analyzed electrophysiological data during stable eye epochs (eye position remained fixed for at least 1 s). This applied to all wake-state data (resting, oddball paradigm and fixation task).

For awake experiments, we monitored monkeys' eye position using a video-based eye tracker (500 Hz sampling rate). For anesthesia experiments, we monitored eyes using a digital video camera (capturing 30 frames per second) and used MATLAB to analyze luminance contrast in a window tightly bounding the eye image. The contrast differentiated closed eyes (i.e., relatively

homogeneous high luminance eyelid shade) and thalamic stimulation-induced eye openings (i.e., dark pupil and iris contrasting against sclera), as shown in Figure 1A; and visual inspection of the eye video verified the timing of eye openings/closings derived from the contrast analysis.

Arousal scoring

We developed an arousal index based on clinical arousal scales to measure the behavioral effects of electrical stimulation. The arousal index incorporated five main indicators of arousal, with each indicator scored 0, 1 or 2, and the sum of the scores of the five indicators yielding the arousal index (range 0-10). The five indicators are:

1) limb/face movements (0 = nothing; 1 = small movement or increased EMG with no clear movement; 2 = full reach or withdrawal)
2) oral signs (0 = nothing; 1 = small mouth/jaw/tongue movements; 2 = full jaw openings/closures, with multiple repetitions)
3) body movements (0 = nothing; 1 = small torso movement or swallowing; 2 = large full torso movement)
4) eye movements/openings (0 = nothing; 1 = eyelid flutters/small blinks or increased eye movements; 2 = full eye opening with occasional blinks)
5) vital signs (0 = no change, i.e., difference of < 10% respiration rate (RR), < 5% heart rate (HR); 1 = difference of > 10% RR, > 5% HR; 2 = at least 20% change in either RR or HR, or at least 10% change in both RR and HR; compared to baseline 30 s prior to stimulation).

A veterinarian at the Wisconsin National Primate Research Center, a clinical anesthesiologist, and five other primate electrophysiologists observed the electrical stimulation effects during anesthesia experiments. Using observations recorded at the time of stimulation experiments as well as offline review of videos and EMG data (filtered 30-450 Hz, full-wave rectified, then filtered 5-100 Hz to extract the envelope), we scored arousal level prior to, during, and after all stimulation events. A typical stimulation block consisted of three stimulation event repetitions (one minute each) within a seven minute recording period at a given site, using the same stimulation frequency, current, polarity, duration, anesthetic and dose. We defined stimulation event epochs from the onset to offset of pulses, i.e., from 1-2 minutes, 3-4 minutes, and 5-6 minutes of a seven minute block. The time between two stimulation epochs was split equally into post- and pre-stimulation epochs (see Figure 1A for an example). The pre-stimulation, during stimulation and post-stimulation arousal index for a block reflected the maximum possible score across the repetitions (repetitions largely produced the same score within each epoch type). Prior to electrical stimulations (except for a rare few instances testing the valence of different stimulation frequencies), the arousal index was 0 or 1. This could be differentiated from stimulation events inducing an arousal index of 3 or more by all observers. Thus, we defined effective stimulation events as those inducing an arousal index of 3 or more, whereas ineffective stimulation events had an arousal index of 0-2. The behavioral indices used to compute the arousal score are based on behaviors exhibited by individuals recovering from general anesthesia or disorders of consciousness. Stimulation-induced arousal scores reflect different (parallel) progressions along the recovery sequence.

Electrophysiological recording and stimulation

FEF and LIP electrodes had either 16 or 24 contacts, and CL electrodes had 24 contacts (MicroProbes). These platinum/iridium electrode contacts had a diameter of 12.5 μm, and 200 μm spacing between contacts. The impedance of contacts on recording electrodes was typically 0.8-1 MΩ. We also measured the EEG using titanium skull screws located above dorsal frontoparietal cortex and, in anesthetized experiments, the EMG using a hypodermic needle (30G) in the forearm. We recorded electrode signals (filtered 0.1-7,500 Hz, amplified and sampled at 40 kHz) using a preamplifier with a high input impedance headstage and OmniPlex data acquisition system controlled by PlexControl software.

We electrically stimulated using 24-contact electrode arrays that had previously been used several times as recording electrodes (and now had lower impedance). In early stimulation trials, we titrated current (tested 100-300 μA, but because 100-200 μA induced arousal, there were only a small number of > 200 μA cases), polarity of first phase of biphasic pulse (negative- or positive-going first phase), number of electrode contacts simultaneously stimulated (tested 1, 4, 8 and 16 contacts), and stimulation duration (15-60 s). For subsequent electrical stimulations, we simultaneously stimulated via 16 electrode contacts (16 most ventral contacts), with 400 μs bi-phasic pulses of 200 μA, for a total of 60 s stimulation duration for any given stimulation event (experiments included multiple stimulation events). We typically performed three stimulation events at a given frequency within a stimulation block for reproducibility, with a recovery time of at least the stimulation event duration between repetitions, i.e., stimulations from 1-2 minutes, 3-4 minutes, and 5-6 minutes of a seven minute block. In our analyses, we included all stimulation data with currents from 100-200 μA. Stimulation event duration, ranging from 15-60 s, did not influence arousal indices, so we included all durations in our analyses.

Electrode array localization

We acquired T1-weighted structural images with electrodes held *in situ* by the customized guide tubes (Pigarev et al., 2009; Saalmann et al., 2007, 2012). While the actual electrode is not visible in the images, a susceptibility "shadow" artifact appears along the length of the electrode with a width of approximately one voxel (0.5 mm^3, either side of the electrode). We targeted electrodes to thalamocortical ROIs based on the individual monkey's structural images, using a stereotaxic atlas as a general reference

(Saleem and Logothetis, 2007). We re-positioned electrodes as necessary and re-acquired T1-weighted structural scans until electrodes were in their desired locations in the thalamus and cortex. Offline, we registered (6 degrees of freedom) the images with electrodes *in situ* to the high-quality structural image acquired prior to surgery. Using measurements of electrode depth during imaging and recording sessions as well as the image of electrodes *in situ*, we reconstructed recording and stimulation sites along electrode tracks. Thalamic stimulation sites, specifically the eighth electrode contact of the 16 contacts simultaneously used for electrical stimulation (i.e., middle of stimulating array), are shown on one coronal slice (sites collapsed across the anterior-posterior axis) in Figure 1 (monkey R).

We further validated the localization of recording sites in our three thalamocortical ROIs using functional criteria. We confirmed the FEF ROI in an initial experiment using electrical stimulation at the frontal recording site, i.e., low currents (< 100 μA) elicited eye movements (Bruce et al., 1985). In the LIP ROI during awake experiments, a large number of neurons showed the classical response characteristic of peri-saccadic activity. In the CL ROI, we found a subset of neurons with high firing rates (around 40-50 Hz) in the awake state, consistent with a CL locus (Glenn and Steriade, 1982; Steriade et al., 1993).

With the aim of positioning electrode contacts in all cortical layers in FEF and LIP, we used depth measurements derived from structural images to initially position electrode arrays across FEF and LIP layers (24 contacts with 200 μm spacing between contacts corresponds to a 4.6 mm span, and 16 contacts correspond to a 3 mm span, which generally allows for contacts in superficial, middle and deep cortical layers for tracks near perpendicular to the cortical surface or with moderate angles from perpendicular). We further adjusted electrode position to maximize the number of contacts showing single-unit or multi-unit spiking activity, and we visualized evoked potentials to auditory tones, with middle layers showing earliest response. We then used current source density (CSD) analysis to attribute contacts to superficial, middle and deep cortical layers (see section "Current Source Density [CSD]" below).

We performed post-mortem histology to reconstruct electrode tracks in one monkey (in addition to the reconstructions using structural MRI and electrode depth measurements in both monkeys). After fixing the brain in 10% neutral buffered formalin, the right hemisphere was cut into approximately 5 mm thick coronal sections, embedded in paraffin, then thinly sectioned (8 μm). Around ROIs, we stained sections with Hematoxylin and Eosin, and visualized sections under a microscope to confirm electrode tracks through our ROIs.

We recorded 282 CL neurons, 281 FEF neurons and 282 LIP neurons in total. For CL, there were 181 neurons during anesthesia; 101 neurons during wakefulness; and 83 neurons during sleep. For FEF superficial, middle and deep layers, there were respectively 48, 33 and 91 neurons during anesthesia; 37, 22 and 50 neurons during wakefulness; and 37, 22 and 42 neurons during sleep. For LIP superficial, middle and deep layers, there were respectively 38, 34 and 91 neurons during anesthesia; 36, 10 and 73 neurons during wakefulness; and 24, 9 and 65 neurons during sleep. Neurons recorded during sleep were also recorded during the wake state. Neurons recorded during anesthesia were recorded in different sessions from neurons recorded during wakefulness/sleep.

Anesthesia experiments

We used either isoflurane (9 sessions: 5 for Monkey R, 4 for Monkey W) or propofol (9 sessions: 4 for Monkey R, 5 for Monkey W) in anesthesia experiments, to ensure that results were not drug-specific, instead reflecting general mechanisms of anesthesia/consciousness. The duration of each anesthesia experimental session was 10-12 hours. We induced anesthesia with ketamine (up to 20 mg/kg body weight, i.m.), then intubated the monkey and inserted an intravenous catheter(s) for fluid and drug administration. We maintained general anesthesia in spontaneously respiring monkeys with isoflurane (0.8%–1.5% on 1 L/min O_2 flow) or propofol (0.17-0.33 mg/kg/min i.v.), and a clinical anesthesiologist (A.R.) oversaw stable conditions throughout. We categorized doses as lower (isoflurane < 1%; propofol < 0.23 mg/kg/min), medium (isoflurane 1%–1.19%; propofol 0.23-0.26 mg/kg/min) and higher (isoflurane ≥ 1.2%; propofol ≥ 0.27 mg/kg/min) within the aforementioned ranges for statistical purposes (see "Quantification and Statistical Analysis" section). We positioned monkeys in the prone position within a modified stereotaxic apparatus atop a surgical table, with the monkey's head immobilized by four rods (attached to the stereotaxic device) that slid into the implant hollows. We maintained the monkey's temperature using a forced-air warming system and monitored vitals (end tidal carbon dioxide, respiration rate, oxygen saturation, heart rate, blood pressure and rectal temperature).

Each experimental session had two parts: the first part involved simultaneous recordings from FEF, LIP and CL (recordings started at least two hours after anesthetic induction and ketamine administration), and the second part involved electrical stimulation of CL during simultaneous recordings from FEF and LIP without changing the anesthetic regimen. We independently positioned linear multielectrode arrays in each ROI, and allowed arrays to settle for 30 minutes prior to starting recordings. Microdrives coupled to an adaptor system allowed different approach angles for each ROI. For both parts of experiments, we interleaved resting state epochs and the passive auditory oddball paradigm. During the first part of the experimental session, we performed neural recordings at a number of different anesthetic levels, adapting the dose to reflect a range of clinically relevant anesthetic depths, e.g., 1%, 1.1%, 1.25% and/or 1.5% isoflurane, or 0.2, 0.225, 0.25 and/or 0.3 mg/kg/min propofol, allowing dosing changes to stabilize before starting the next block of recordings (typically at least 30 minutes). During the second part of the experiment, we either electrically stimulated using the linear multielectrode array existing in the thalamus or replaced it with another array inserted along the same trajectory to the same depth. We first stimulated thalamic sites at a frequency of 50 Hz. If this did not induce arousal, then we moved the stimulating electrode to a new depth in the thalamus in steps of 0.5-1 mm dorsal or ventral along the electrode track, until stimulation induced arousal. When 50 Hz stimulation induced arousal, we tested additional stimulation frequencies, i.e., 2, 10 or 200 Hz, or further depths (mapping the area of effect). The order of stimulation frequencies generally followed one of two patterns: 50 Hz alternating

with one of the other stimulation frequencies; or multiple repetitions of a particular stimulation frequency, followed by multiple repetitions of a different stimulation frequency.

In early experiments, we tested thalamic stimulations at different anesthetic doses between 0.8%–1.3% for isoflurane and between 0.17-0.3 mg/kg/min for propofol. We observed thalamic stimulation-induced arousal for all but the highest doses (i.e., 1.3% isoflurane and 0.3 mg/kg/min propofol). In subsequent isoflurane experiments, we used doses between 0.8 – 1.25% (M = 1.04, SD = 0.11) during thalamic stimulation, and in propofol experiments, we used doses between 0.17-0.28 mg/kg/min (M = 0.23, SD = 0.03). Data for all doses were included in analyses and controlled for statistically (see "Quantification and Statistical Analysis" section).

As an additional control, we also separately stimulated the FEF and LIP using the same stimulation parameters as those used in the thalamus (10 or 50 Hz). FEF or LIP stimulation alone did not induce arousal. Stimulating both areas would have required considerable piloting and additional experimentation, and was thus beyond the scope of this study.

Awake experiments

We performed 40 awake experimental sessions (18 for monkey R; 22 for monkey W), each session usually of 2-4 hours duration. Monkeys sat upright in a primate chair with their head immobilized using the head post and/or four rods that slid into the hollow slots in the head implant. Awake experiments were split into two types (similar to the two parts of anesthesia experimental sessions); those with and without thalamic stimulation. Experiments without stimulation involved simultaneous recordings from FEF, LIP and CL across multiple blocks of all task conditions. Stimulation experimental sessions involved electrical stimulation of CL, at different frequencies, during simultaneous recordings from FEF and LIP across all task conditions. During each type of experiment, we interleaved task conditions involving reward (fixation and oddball fixation) with those not involving rewards (resting state and passive oddball). The specific task order was varied randomly across different experimental sessions.

For electrical stimulation, we pseudorandomly applied stimulation blocks of different frequencies, i.e., 10, 50 and 200 Hz. Because electrical stimulation of the thalamus at 50 Hz frequency (or other frequencies) in awake monkeys did not elicit any movements (as observed during effective stimulation events in anesthesia experiments), it is unlikely that the effects of 50 Hz stimulation of CL in anesthetized monkeys simply reflected direct effects on the motor system. Rather, it supports the finding that 50 Hz stimulation effects reflected increased arousal.

We performed neural recordings from brain areas implicated in awareness. Because these areas are also involved in selective attention and oculomotor function, we aimed to ensure differences between wake and anesthesia results were not related to attentional or saccadic processes. To this end, within the wake state, we compared recordings during the fixation task to resting state, as well as recordings during the passive oddball with fixation to that without fixation. For each condition (fixation task, resting state, oddball with and without fixation), we analyzed epochs (at least 1 s in duration) in which the monkey's eye position was stable, as verified using the eye tracker. These analyses showed neural data from compared conditions to be qualitatively similar. Considering these controls, to keep wake and anesthesia conditions as similar as possible, we compared wake and anesthesia data collected during conditions in which there were no task demands, i.e., the resting state and passive oddball conditions (not the fixation task or the oddball with fixation) in the dark.

Sleep

During awake experiments, monkeys at times would fall asleep, particularly during conditions not involving rewards, such as the resting state. Online, we identified non-rapid eye movement (NREM) sleep using the following criteria: increased delta (1-4 Hz) activity in EEG (compared with wake); extended eye closure (recording times when eyes closed and re-opened, to compare with semi-automatic detection offline); preceding period of drowsiness indicated by slow drooping/closing of eyelids; stop in fixation task performance (if current task is fixation task); and no overt body movement. Offline, we identified NREM sleep periods using EEG and eye tracker data. We bandpass filtered (1-4 Hz; Butterworth, order 6) EEG data and applied the Hilbert transform, to calculate the instantaneous delta-band amplitude. From the resulting time series, we detected times of relatively high delta amplitude using thresholds titrated for each recording session, because the mean delta amplitude and standard deviation could vary depending on the recording session and total sleep time. For each session, we selected the threshold as the number of standard deviations from the mean delta amplitude that produced a total sleep time estimate that closely resembled the expected sleep time based on online NREM identification, as well as the offline calculation of the total time when the monkey's eyes were closed (using the recorded eye tracker time series data). Offline NREM sleep identification and time stamping then involved automated detection of extended epochs across the recording session when both the monkey's eyes were closed and delta amplitude was above threshold. These offline NREM sleep detections were similar to manual online detections, and proved reliable for different recording sessions and monkeys.

The identified sleep epochs corresponded to early phases of NREM sleep (N1 or N2, i.e., light sleep). Thus, monkeys were not at the same depth of unconsciousness during sleep as they were during general anesthesia in our study. This notwithstanding, we included the spike rate data during early NREM sleep, as this allowed us to compare the influence of conscious and less-conscious states on the same subset of neurons (n = 282) recorded in both wakefulness and sleep. This further substantiated our comparison of spiking activity between the awake and anesthetized states, activity recorded from two different samples of neurons from the same ROIs (maintenance of stable anesthesia up to 12 hours required recordings to take place in a surgical suite, whereas awake

recordings took place in the behavioral lab). Because local field potentials (LFPs) reflect combined activity from a considerably larger volume (compared with single-neuron activity) (Katzner et al., 2009), LFPs recorded at different times, i.e., awake and during anesthesia, are more readily compared. Nonetheless, we include early NREM sleep LFP data as well, to further substantiate the altered connectivity during anesthesia (although a complete account of sleep influence on our thalamocortical recordings is beyond the scope of this study).

Neural data preprocessing

We defined data segments of 1 s duration (akin to trials) for analysis. In the awake state, we first determined stable eye epochs (to match eye behavior between conscious and unconscious states), i.e., epochs starting 200 ms after a saccade and ending 200 ms before the next saccade. Next, we divided stable eye epochs into non-overlapping 1 s windows. In the anesthetized and non-REM sleep states (when eyes are closed), we divided all data in each of these states into non-overlapping 1 s windows.

We lowpass filtered data to 250 Hz for LFPs (Butterworth, order 6, zero-phase filter). Next, we linearly detrended LFPs, then extracted artifacts from LFP data, by removing significant sine waves using the Chronux function rmlinesc. Individual electrode contacts with signal amplitude greater than 5 standard deviations from the mean were excluded from analysis. For power and coherence analyses, we further calculated bipolar derivations of LFPs, i.e., the difference between two adjacent electrode contacts (excluding contacts that had been removed due to noise), to minimize any possible effects of a common reference and volume conduction (Bollimunta et al., 2008; Haegens et al., 2015; Trongnetrpunya et al., 2016).

We bandpass filtered data 250-5,000 Hz for spiking activity (Butterworth, order 4, zero-phase filter) and sorted spikes using Plexon Offline Sorter software. Initial spike detection involved thresholding data at > 3 standard deviations away from the mean. We then used principal components analysis to extract features of the spike shapes. Finally, we used the T-distribution expectation maximization algorithm to identify clusters of spikes with similar features.

For neural data during electrical stimulation, there was a brief artifact caused by the applied current. To remove this artifact, we first excised a 1 ms window around the artifact, then linearly interpolated across this window. Next, we used the Chronux function rmlinesc to remove any significant sine waves at the stimulation frequency (we also performed artifact removal using the SARGE toolbox (Erez et al., 2010), which yielded qualitatively similar results).

Spike rate

We calculated the average spike rate in 1 s windows (during stable eye epochs) for each neuron, in the awake, sleep and/or anesthetized states. We divided anesthetized state data into electrical stimulation and no stimulation windows. For electrical stimulation data, we calculated the spike rate during the stretches of data unaffected by the stimulation-induced artifact.

Spike timing

For each neuron, we generated interspike interval (ISI) histograms (1 ms bin width), from which we derived an index of burst firing propensity in the awake and anesthetized states (Senzai et al., 2019). We excluded neurons with very low spike rate (< 1 Hz) from the burst index analysis, as their ISI histograms had too few samples). For thalamic neurons, the burst index equaled the proportion of spikes occurring within 2-8 ms (sum of spikes in the 2-8 ms bins of the ISI histogram divided by the total number of spikes; Figure 2D); we also calculated indices for 2-5, 2-10 and 2-15 ms bins (for qualitatively similar results). Because ISIs in CL neuronal bursts have been reported to commonly range up to 6 ms (lengthening with increasing burst size) (Lacey et al., 2007), we selected the next accommodating window size, 2-8 ms. For cortical neurons, the burst index equaled the proportion of spikes occurring within 2-15 ms (sum of spikes in the 2-15 ms bins of the ISI histogram divided by the total number of spikes; Figure 2E); we also calculated indices for 2-10, 2-20 and 2-30 ms bins. Although it has been reported that LIP neurons have a low tendency to burst in the wake state (Maimon and Assad, 2009), we still measured changes in spiking regularity across different states, by using a relatively larger window, 2-15 ms (*cf.* CL), still applicable for frontal cortex (Womelsdorf et al., 2014), to allow comparisons between cortical areas.

Current source density (CSD)

We localized electrode contacts to superficial, middle or deep cortical layers based on inverse CSD analyses (Pettersen et al., 2006). To do this, we used the CSDplotter toolbox for MATLAB (https://github.com/espenhgn/CSDplotter; dt = 1 ms, cortical conductivity value = 0.4 S/m, diameter = 0.5 mm) for calculating the inverse CSD in response to auditory tones in the passive oddball paradigm. Linear multi-electrode arrays measure the LFP, ϕ, at N different cortical depths/electrode contacts along the z axis with spacing h. The standard CSD, C_{st}, is estimated from the LFPs using the second spatial derivative.

$$C_{st}(z) = \frac{(\phi(z+h) - 2\phi(z) + \phi(z-h))}{h^2}$$

LFPs can also be estimated from given CSDs, represented in matrix form as $\Phi = F\widehat{C}$, where Φ is the vector containing the N measurements of ϕ, $\widehat{C}$ is the vector containing the estimated CSDs, and F is an NxN matrix derived from the electrostatic forward calculation of LFPs from known current sources. The inverse CSD method uses the inverse of F to estimate the CSD, i.e., $\widehat{C} = F^{-1}\Phi$. For the step

inverse CSD method (Pettersen et al., 2006) used here, it is assumed that the CSD is stepwise constant between electrode contacts, so the sources are extended cylindrical boxes with radius R and height h. In this case, F is given by:

$$F_{ji} = \int_{z_i-\frac{h}{2}}^{z_i+\frac{h}{2}} \frac{1}{2\sigma}\left(\sqrt{(z_j - z')^2 + R^2} - |z_j - z'|\right)dz'$$

where σ is the electrical conductivity tensor, and $\phi(z_j)$ is the potential measured at position z_j at the cylinder center axis due to a cylindrical current box with CSD, C_i, around the electrode position z_i. The inverse CSD method offers advantages over the standard CSD. The inverse CSD method estimates the CSD around all N electrode contacts, whereas the standard CSD method yields estimates around N-2 contacts. Further, the standard CSD requires equidistant contacts, whereas the inverse CSD method does not, which is advantageous when data from a noisy contact may need to be excluded. We used the step inverse CSD method, because it may perform better than the delta-source CSD method as electrode contact spacing increases, and the spline CSD method can be more sensitive to spatial noise, e.g., from gain differences between electrode contacts or from an excluded contact (Pettersen et al., 2006).

We identified the early current sink in response to auditory stimulation and designated the bottom of the sink as the bottom of the middle layers (around boundary between layers 4 and 5). We included the electrode contact at the bottom of the middle layers and the two more superficial contacts as the middle layers. Electrode contacts in FEF or LIP superficial to the middle layers were designated as being in the superficial layers, whereas FEF or LIP contacts deeper than the middle layers were designated as being in the deep layers. Layer assignments were cross-referenced to reconstructions of the recording sites along the electrode track (based on measurements of electrode depth as well as the image of electrodes *in situ*) as well as to single-unit or multi-unit spiking activity, which helped delineate the border between gray and white matter. We excluded from analysis contacts that were found to be located outside the ROI.

Previous studies generated CSD data in FEF (Chen et al., 2018) and LIP (Schroeder et al., 1998) using visual stimulation (FEF: 1 degree of visual angle square at 60% contrast; LIP: diffuse light). Our CSD profiles generated with auditory stimulation were roughly consistent with these previous studies of FEF and LIP in so far as sensory stimulation elicited early sinks in middle layers (which would be predicted based on auditory stimulation activating middle cortical layers relatively early).

We also performed CSD analyses, in the case of resting state recordings, using LFP signals aligned to the trough of delta-band oscillations recorded from the electrode contact with the highest delta power (i.e., this contact served as the phase index) (Bollimunta et al., 2008; Funk et al., 2016; Haegens et al., 2015). These delta phase-realigned CSDs showed differences across cortical layers which helped verify that probe positions remained stable across recording blocks that did not include auditory stimuli of the passive oddball paradigm.

Power

We calculated power in 1 s windows (stable eye epochs) for every bipolar-derived LFP, using multi-taper methods (5 Slepian taper functions, time bandwidth product of 3, averaging over windows/trials) with the Chronux data analysis toolbox for MATLAB (http://chronux.org/) (Bokil et al., 2007, 2010; Mitra and Bokil, 2007). Noisy trials, samples with amplitudes that exceeded 4 standard deviations from the mean, were removed. Sinusoidal noise, especially at stimulation frequencies and 60 Hz, was removed using notch filters or the Chronux function rmlinesc. There were an unequal number of windows per condition, due to differences in data length and number of stable eye epochs. Because the number of time windows (or trials) affects the power estimate (S(f)), we bias-corrected power values (Bokil et al., 2007). The bias-corrected power spectrum, B(f), is given by:

$$B(f) = \log(S(f)) - \psi\left(\frac{v_0}{2}\right) + \ln\left(\frac{v_0}{2}\right)$$

where $v_0 = 2*K*N$, where K is the number of tapers (5) and N is the number of time windows. To obtain population values, we pooled the bias-corrected power estimates for the awake state and again for the anesthetized state (separately for the no stimulation, effective stimulation and ineffective stimulation conditions).

Coherence

We calculated coherence using multi-taper methods (5 Slepian taper functions, time bandwidth product of 3) with the Chronux toolbox. Noisy trials, samples with amplitudes that exceeded 4 standard deviations from the mean, were removed. Sinusoidal noise, especially at stimulation frequencies and 60 Hz, was removed using notch filters or the Chronux function rmlinesc. We used the coherence measure to study the temporal relationship between LFPs, or between spikes and LFPs, within and between the thalamus, FEF and LIP. The coherence is given by:

$$C(f) = \frac{S_{12}(f)}{\sqrt{(S_{11}(f)S_{22}(f))}}$$

where S(f) is the spectrum with subscripts 1 and 2 referring to the simultaneously recorded spike/LFP at one site and LFP at another site. The coherence is normalized between 0 and 1, so it can be averaged across different pairs of time series. For each paired

recording, we calculated the coherence in 1 s windows during which the monkey's eyes were stable. There were an unequal number of windows per condition, due to differences in data length and number of stable eye epochs. Because the number of time windows (or trials) affects the coherence estimate, we bias-corrected/transformed coherence values (Bokil et al., 2007). The transformed coherence, T(f), is given by:

$$T(f) = \tanh^{-1}(C(f)) - \frac{1}{(v_0 - 2)}$$

where ν_0 is the degrees of freedom; for our multi-taper estimates, $\nu_0 = 2*K*N$, where K is the number of tapers (5) and N is the number of time windows. To obtain population values, we pooled the transformed coherence estimates for the awake state and again for the anesthetized state (separately for the no stimulation, effective stimulation and ineffective stimulation conditions).

To ensure that changes in coherence did not simply reflect changes in power at given frequency bands, we investigated the relationship between our power and coherence results. While we did find that anesthesia increased delta power and decreased power at higher frequencies for all cortical areas, power changes during thalamic stimulation were broadband and typically smaller for effective relative to ineffective stimulations (unlike coherence changes; Figure S3; Table S2). This poor correlation between arousal and power during stimulation suggests that power is unlikely to be driving stimulation-induced changes in coherence, and is not a key component of the NCC.

QUANTIFICATION AND STATISTICAL ANALYSIS

General approach

We performed statistical analyses using general linear models (GLMs) in R via RStudio, regressing the relevant dependent variable on all independent variables, interactions, and covariates (Models 1-21 below). We used linear models (LM in R) for effects that varied between all other effects, yielding T statistics for each estimated slope (β parameter). Effects that varied within other effects of interest were estimated using linear mixed effect models (LMER in R), yielding F statistics, or after computing difference scores with linear models, yielding T statistics. Random effects of LMER models are represented as gamma parameters, and all simple and main effects are presented as beta parameters, where the slope for the effect of interest is β_1. P values stemming from the same family of statistical tests (models intended to describe the same effect in different populations) were controlled for multiple comparisons using Holm's correction.

To compare doses between anesthetics, we separated doses into lower (-1), medium (0), and higher (1) dose groups within the experimental range used for both anesthetic agents. For isoflurane, lower doses were $< 1\%$, medium were $\geq 1\%$ and $< 1.2\%$, and higher doses were $\geq 1.2\%$. For propofol, lower doses were < 0.23 mg/kg/min, medium were ≥ 0.23 and < 0.27 mg/kg/min, and higher doses were ≥ 0.27 mg/kg/min. This allowed us to use coded dose (DoseCode) as a covariate independent of anesthetic.

To contrast stimulation effectiveness, we coded stimulations producing arousal ≥ 3 as effective (1) and those producing arousal < 3 as ineffective (0). This allowed us to compare neural dynamics across stimulations that reflected clear changes in the level of consciousness while controlling for changes that may be induced only by introduction of thalamic current, which was the same for ineffective and effective stimulations.

To limit the number of multiple comparisons across frequency, we averaged power and coherence across canonical frequency bands: delta = 0-4 Hz, theta = 4-8 Hz, alpha = 8-15 Hz, beta = 15-30 Hz, low gamma = 30-60 Hz and high gamma = 60-90 Hz. As a control for possible artifacts, we also averaged more selectively within the low gamma (across 30-47 and 53–57 Hz) and high gamma (63-90 Hz) bands, so as not to include data at 50 Hz, the frequency of thalamic stimulation, and 60 Hz, the frequency of power line noise, producing similar results.

Stimulation effects

To test the general effect of thalamic stimulation on arousal (Figure 1B), we regressed arousal score within stimulation blocks on the peri-stimulation epoch (pre, stimulation, post), including dose and anesthetic as covariates. Peri-stimulation epoch (StimEpochF) was dummy coded as a factor referenced to the epoch with stimulation, anesthetic was coded as a centered dichotomous variable (isoflurane = -0.5, propofol = 0.5), and dose was treated as DoseCode. We included random slopes only for stimulation epochs, as dose and anesthetic remained constant within a given stimulation event. Significantly negative β_1 shows that outside of stimulation, arousal score is lower even controlling for the effects of dose and anesthetic.

$$ArousalScore \sim \beta_0 + \beta_1 * StimEpochF + \beta_2 * DoseCode + \beta_3 * Anes \quad \text{(Model 1)}$$

To ensure the effects of stimulation were not being driven or modulated by dose, we repeated this model using DoseCode as an interactant, but the interaction was not significant (Figures S1A–S1C).

To test the effect of dorsal-ventral (D-V) proximity to CL of the stimulation array on arousal (Figure 1F), we regressed the stimulation arousal difference (stim – pre) on the linear and quadratic components of the D-V proximity to CL of the centermost contact of each stimulation array, including dose, anesthetic, and variation of placement along the medial-lateral (M-L) axis as covariates. D-V distance (D-Vdist) was coded as the distance from the centermost contact of the stimulation array to center of CL in the D-V plane in each monkey, dose was coded as DoseCode, anesthetic (Anes) was coded as a dichotomous variable

(isoflurane = −0.5, propofol = 0.5), and M-L distance (M-Ldist) was coded as the linear distance from the centermost contact in the stimulation array to the center of CL in the M-L plane for each animal. Significantly negative β_1 shows that moving more dorsal or more ventral from the center of CL decreases the arousal induced by stimulation above and beyond the effects of anesthetic, dose, and M-L variation.

$$AwakeDiff(stim - pre) \sim \beta_0 + \beta_1 * D - Vdist^2 + \beta_2 * D - Vdist + \beta_3 * DoseCode + \beta_4 * M - Ldist + \beta_5 * Anes \quad \text{(Model 2)}$$

To test the effect of Euclidian distance from the center of CL on arousal (Figures S1G–S1I), we regressed arousal difference (stim – pre) on the Euclidian distance (Distance) including dose, anesthetic, and monkey as covariates. Importantly, we included monkey as a covariate in this model to control for general differences between the monkeys in terms of the size and shape of their anatomy in M-L and D-V planes (main source of variation in our electrode track locations). Euclidian distance was calculated as the length of a vector from the center of CL to the centermost contact of each stimulation array. Dose was coded as DoseCode, anesthetic (Anes) was coded as a centered, dichotomous variable (isoflurane = −0.5, propofol = 0.5), and monkey (Animal) was coded as a centered, dichotomous variable (monkey R = −0.5, monkey W = 0.5). Significantly negative β_1 shows that moving further from the center of CL in any M-L/D-V direction decreases the arousal induced by stimulation above and beyond variation contributed by dose, anesthetic, or monkey.

$$AwakeDiff(stim - pre) \sim \beta_0 + \beta_1 * Distance + \beta_2 * DoseCode + \beta_3 * Anes + \beta_4 * Animal \quad \text{(Model 3)}$$

To test the relative effectiveness of stimulation frequency on arousal (Figure 1H), we regressed arousal difference (stim – pre) on stimulation frequency, for all case-matched examples in which stimulations occurred at the same site, at multiple frequencies, and at least one stimulation had been effective (arousal score ≥ 3). Because only 50 Hz stimulations reliably increased arousal (Figure 1H; error bars did not include 0), we coded stimulation frequency (StimFreq) as a dichotomous variable, where stimulations were either at 50 Hz (0.5) or not at 50 Hz (−0.5). Dose (DoseCode) was coded as a factor reflecting lower, medium and higher doses within our experimental range, and anesthetic (Anes) was coded as a centered dichotomous variable (isoflurane = −0.5, propofol = 0.5). Significantly positive β_1 shows that, as monkeys go from pre to stimulation conditions, arousal increases more when stimulations are at 50 Hz above all other frequencies, even controlling for differences in dose and anesthetic between stimulation blocks.

$$AwakeDiff(stim - pre) \sim \beta_0 + \beta_1 * StimFreqB + \beta_2 * DoseCode + \beta_3 * Anes \quad \text{(Model 4)}$$

Spike rate effects

For non-stimulation data, we limited all comparisons to resting state and anesthesia conditions without auditory stimuli. To test the effect of sleep on thalamic spike rate (Figure 2C), we regressed spike rate within neuron on state (wake versus sleep). State was coded as a dichotomous variable (wake = 0, sleep = 1). A random intercept and slope for state was included by neuron. Significant negative β_1 shows that after neurons transition from wake to sleep, spike rate tends to decrease.

$$SpikeRate \sim \beta_0 + \beta_1 * State + \gamma_{neuron} * (1 + State) \quad \text{(Model 5)}$$

In the cortex (Figures 2F–2H), we used a similar model but included the layer from which the neuron was recorded (SpikeLayer) as an interaction. SpikeLayer was dummy coded as a factor referenced to the deep cortical layers. A random intercept and slope for state was included by neuron. No random slope was included for spike layer as it could not vary within neuron. Finding significant positive β_1 for the interaction of state and layer shows that the decrease in spike rate predicted by the state change is less for superficial relative to deep cortical layers controlling for variation in the middle layer spike rate. This model was used separately for neurons found in FEF and LIP (and controlled for multiple comparisons).

$$SpikeRate \sim \beta_0 + \beta_1 * State * SpikeLayer + \beta_2 * State + \beta_3 * SpikeLayer + \gamma_{neuron} * (1 + State) \quad \text{(Model 6)}$$

To test the effect of anesthesia on thalamic spike rate (Figure 2C), we regressed spike rate between neuron on state (wake versus anesthesia). State was coded as a dichotomous variable (wake = 0, anesthesia = 1). Significant β_1 shows that neurons recorded during anesthesia had lower spike rates relative to wakefulness.

$$SpikeRate \sim \beta_0 + \beta_1 * State \quad \text{(Model 7)}$$

In the cortex (Figures 2F–2H), we used a similar model but included the layer from which the neuron was recorded (SpikeLayer) as an interaction. SpikeLayer was dummy coded as a factor referenced to the deep cortical layers. Finding significant positive β_1 for the interaction of state and layer shows that the decrease in spike rate predicted by the state change is less for superficial relative to deep cortical layers controlling for variation in the middle layer spike rate. This model was used separately for units found in FEF and LIP.

$$SpikeRate \sim \beta_0 + \beta_1 * State * SpikeLayer + \beta_2 * State + \beta_3 * SpikeLayer \quad \text{(Model 8)}$$

To ensure that effects were consistent between anesthetics, we compared the spike rate for each type of neuron (superficial, middle, deep cortical, or thalamic) separately across anesthetic states (isoflurane versus propofol; Figures S2A–S2D) including dose and cortical area as covariates. State was dummy coded as a dichotomous variable (propofol = 0, isoflurane = 1). Cortical area (Area) was coded as a centered dichotomous variable (FEF = −0.5, LIP = 0.5) and dose was coded as DoseCode. Negative β_1 shows

that spikes recorded during isoflurane have lower spike rate than those recorded under propofol (though none were significant after controlling for multiple comparisons).

$$SpikeRate \sim \beta_0 + \beta_1 * StateF + \beta_2 * Area + \beta_3 * DoseCode \quad \text{(Model 9)}$$

For stimulation data, we analyzed passive auditory oddball paradigm data in addition to resting state data. To test the effect of thalamic stimulation (50 Hz) on cortical spike rate (Figures 1I–1K), we regressed spike rate within stimulation block on the 4-way interaction between peri-stimulation epoch (pre versus stim), cortical layer (superficial versus deep), stimulation effect (effective versus ineffective), and cortical area (FEF versus LIP), including dose, anesthetic and task as covariates. Peri-stimulation epoch (StimEpoch) was coded as a dichotomous variable (pre = −1, stim = 0), spike layer (SpikeLayer) was coded as a dichotomous variable (superficial = 0, deep = 1), stimulation effectiveness (StimEffect) was coded as a dichotomous variable (ineffective = 0, effective = 1), and cortical area (Area) was coded as a centered dichotomous variable (FEF = −0.5, LIP = 0.5). In addition, dose was coded as DoseCode, and anesthetic (isoflurane = −0.5, propofol = 0.5) and task (resting state = −0.5, passive oddball = 0.5) were coded as a centered, dichotomous variables. A random intercept and slope for stimulation epoch was included by stimulation block (stimID), as this was the only variable which changed within a given stimulation block. A significantly positive β_1*for the 4-way interaction shows that effective stimulation increases spike rate more for deep layers in LIP than any other condition, controlling for differences in dose, anesthetic, and task conditions.

$$\begin{aligned} SpikeRate \sim\ & \beta_0 + \beta_1 * StimEpoch * SpikeLayer * StimEffect * Area + \beta_2 * StimEpoch * StimEffect * Area + \\ & \beta_3 * StimEpoch * SpikeLayer * Area + \beta_4 * StimEpoch * SpikeLayer * StmEffect + \\ & \beta_5 * SpikeLayer * StimEffect * Area + \beta_6 * StimEpoch * SpikeLayer + \beta_7 * StimEpoch * StimEffect + \\ & \beta_8 * StimEpoch * Area + \beta_9 * SpikeLayer * StimEffect + \beta_{10} * SpikeLayer * Area + \beta_{11} * StimEffect * Area + \\ & \beta_{12} * StimEpoch + \beta_{13} * SpikeLayer + \beta_{14} * StimEffect + \beta_{15} * Area + \beta_{16} * DoseCode + \beta_{17} * Anes + \beta_{18} * task + \\ & \gamma_{stimID} * (1 + StimEpoch) \end{aligned} \quad \text{(Model 10)}$$

Bursting effects

To test the effect of sleep on thalamic bursting (Figure 2D), we regressed bursting index within neuron ($BI_{2\text{-}8}$; derived from the 2-8 ms bins of the ISI histogram) on state (wake versus sleep), including spike rate as a covariate (as spike rate tended to change with state in thalamic neurons and could influence the burst index). State was coded as a dichotomous variable (wake = −0.5, sleep = 0.5). Because the relationship between bursting changes and spike rate was largely linear within neuron, spike rate was coded as a continuous variable (total spikes/total time). We included a random slope for state and spike rate by neuron. A significant positive β_1 indicates that after transitions from wakefulness into NREM sleep, thalamic neurons increase bursting, controlling for changes in spike rate.

$$BI_{2-8} \sim \beta_0 + \beta_1^* State + \beta_2^* SpikeRate + \gamma_{neuron} * (State + SpikeRate) \quad \text{(Model 11)}$$

To test the effect of anesthesia on thalamic bursting (Figure 2D), we regressed bursting index ($BI_{2\text{-}8}$; derived from the 2-8 ms bins of the ISI histogram) between neuron on state (wake versus anesthesia), including spike rate as a covariate (as spike rate tended to change with state in thalamic cells and could influence the burst index). State was coded as a dichotomous variable (wake = 0, anesthesia = 1). As the relationship between bursting changes and spike rate were not reliably linear between neurons, spike rate was log transformed (SpikeRateL) and coded as a continuous variable (ln(total spikes/total time)). A significant positive β_1 indicates that neurons recorded during anesthesia have higher burst index than wakefulness, controlling for differences in spike rate.

$$BI_{2-8} \sim \beta_0 + \beta_1 * State + \beta_2 * SpikeRateL \quad \text{(Model 12)}$$

To test the effect of anesthesia on cortical bursting (Figure 2E), we regressed bursting index ($BI_{2\text{-}15}$; derived from the 2-15 ms bins of the ISI histogram) between neuron on the interaction of state (wake versus anesthesia) and spike layer, including spike rate and cortical brain area as covariates. State (wake = 0, anesthesia = 1) and spike layer (superficial = 0, deep = 1) were coded as dichotomous variables. As both cortical areas yielded similar results, we combined data across the cortex, and included cortical area as a centered, dichotomous covariate (FEF = −0.5, LIP = 0.5). Because the relationship between bursting changes and spike rate were not reliably linear between cells, spike rate was log transformed (SpikeRateL) and coded as a continuous variable (ln(total spikes/total time)). Significant positive β_1 for the state and layer interaction indicates that the increased bursting during anesthesia is larger for deep relative to superficial neurons, controlling for differences in spike rate and cortical area.

$$BI_{2-15} \sim \beta_0 + \beta_1 * State * SpikeLayer + \beta_2 * State + \beta_3 * SpikeLayer + \beta_4 * SpikeRateL + \beta_5 * Area \quad \text{(Model 13)}$$

Power and coherence effects

For the purpose of graphical representation, we computed 95% confidence intervals for power and coherence spectra using the ttest function in MATLAB (reflecting 95% confidence intervals of the mean) for all spectra and paired difference scores (wake – sleep, stim – pre). Similarly, we used the ttest2 function to produce confidence intervals for unpaired difference scores (wake – anesthesia).

To illustrate regions of significant difference across frequencies between states and stimulation conditions, we computed t tests between spectra using the ttest2 command in MATLAB at each frequency. P values were controlled for multiple comparisons using Holm's correction.

We limited all non-stimulation comparisons to resting state and anesthesia conditions without auditory stimuli. To test the effects of anesthetics on power and coherence (Figures S2, S3, and S4), we regressed power (S), coherence (C), and spike-field coherence (spikeFC) averaged across different frequency bands (delta, alpha, theta, beta, low gamma and high gamma) and isolated to different electrode contact pairs of interest (in the case of coherence, e.g., isolated to superficial-deep contact pairs within a cortical area, or deep FEF-deep LIP contact pairs), on state (wake versus anesthesia). For coherence estimates within or between layers of the same cortical layer, we included cortical area as a covariate. Thalamocortical comparisons were performed separately for each cortical area, and thus did not need this covariate. Similarly, cross-area corticocortical coherence, which was always computed between FEF and LIP, did not include this covariate. State was coded as a dichotomous variable (anesthesia = 1, wake = 2), and cortical area (Area) was coded as a centered, dichotomous variable (FEF = −0.5, LIP = 0.5) where applicable. Because spike-field coherence was calculated between individual neurons and derivatized LFPs, we included a random intercept by neuron (this inclusion changed neither the direction nor significance of the effects). Significant positive β_1 parameters show frequency bands with increased power, coherence, or spike-field coherence during wakefulness relative to anesthesia. Significant negative β_1 parameters show frequency bands with decreased power, coherence, or spike-field coherence during wakefulness relative to anesthesia.

Intracolumnar and thalamocortical:

$$C_{(\delta,\theta,\alpha,\beta,\gamma l,\gamma h)} \sim \beta_0 + \beta_1 * State + \beta_2 * Area \qquad \text{Table S1 (Model 14)}$$

$$S_{(\delta,\theta,\alpha,\beta,\gamma l,\gamma h)} \sim \beta_0 + \beta_1 * State + \beta_2 * Area \qquad \text{Table S2 (Model 15)}$$

Cross-area corticocortical:

$$C_{(\delta,\theta,\alpha,\beta,\gamma l,\gamma h)} \sim \beta_0 + \beta_1 * State \qquad \text{Tables S3 and S4 (Model 16)}$$

$$S_{(\delta,\theta,\alpha,\beta,\gamma l,\gamma h)} \sim \beta_0 + \beta_1 * State \qquad \text{Table S2 (Model 17)}$$

$$spikeFC_{(\delta,\theta,\alpha,\beta,\gamma l,\gamma h)} \sim \beta_0 + \beta_1 * State + \gamma_{neuron} * (1) \qquad \text{Tables S3 and S4 (Model 18)}$$

We limited all stimulation comparisons to anesthesia conditions without auditory stimuli where the stimulation frequency was 50 Hz and within the effective current range (120 - 200 μA). To test the effects of 50 Hz thalamic stimulation on power and coherence (Figures 3K–3P, 4F–4H, and S3K–S3P), we regressed change in power (S) and coherence (C) (stim – pre) averaged across different frequency bands (delta, alpha, theta, beta, low gamma, high gamma) and isolated to different electrode contact pairs of interest (in the case of coherence), on stimulation effectiveness (effective versus ineffective) including anesthetic and dose as covariates. For coherence estimates within or between layers of the same cortical layer, we included cortical area as a covariate. Cross-area corticocortical coherence, which was always computed between FEF and LIP, did not include this covariate. Anesthetic (Anes; isoflurane = −0.5, propofol = 0.5) and cortical area (Area; FEF = −0.5, LIP = 0.5), where applicable, were coded as centered, dichotomous variables. We coded dose as DoseCode. Significant positive β_1 parameters show an interaction with stimulation epoch, where positive changes in power or coherence at the given frequency band are significantly larger for effective relative to ineffective stimulations. Significant negative β_1 parameters show changes in power or coherence at the given frequency band that are significantly smaller for effective relative to ineffective stimulations. It was possible to get negative interactions even if power or coherence still increased during stimulation relative to the pre epoch.

Intracolumnar:

$$CDiff_{(\delta,\theta,\alpha,\beta,\gamma l,\gamma h)}(stim - pre) \sim \beta_0 + \beta_1 * StimEffect + \beta_2 * DoseCode + \beta_3 * Anes + \beta_4 * Area \qquad \text{Table S1 (Model 19)}$$

$$SDiff_{(\delta,\theta,\alpha,\beta,\gamma l,\gamma h)}(stim - pre) \sim \beta_0 + \beta_1 * StimEffect + \beta_2 * DoseCode + \beta_3 * Anes + \beta_4 * Area \qquad \text{Table S2 (Model 20)}$$

Cross-area corticocortical:

$$CDiff_{(\delta,\theta,\alpha,\beta,\gamma l,\gamma h)}(stim - pre) \sim \beta_0 + \beta_1 * StimEffect + \beta_2 * DoseCode + \beta_3 * Anes \qquad \text{Table S3 (Model 21)}$$

We considered effects consistent between (a) wake versus anesthesia and (b) effective versus ineffective stimulation comparisons (Figures 3 and 4, gray shading) if both the StimEpoch effect from stimulation models (β_0; stim – pre) were consistent in direction

and significance to the beta parameter for the state effect in non-stimulation models (β_1*State; wake – anesthesia). Such a finding indicates that the changes following stimulation-induced arousal are in the same direction as those found in the wake state over anesthesia. Additionally, the interaction term for stimulation data (β_1*StimEffect) had to be significant, indicating that similarities were limited to the effective stimulation condition, and thus driven by arousal and not applied thalamic current in itself.

DATA AND CODE AVAILABILITY

All data and code available upon reasonable request. Requests should be made to, and will be fulfilled by, the Lead Contact, Yuri B. Saalmann (saalmann@wisc.edu).